Small extracellular vesicles facilitate epithelial-mesenchymal transition in chronic rhinosinusitis with nasal polyps via the miR-375-3p/QKI axis*

Xinyue Wang[1,2,$], Rui Zheng[1,2,$], Weicheng Liang[3,4], Huijun Qiu[1,2], Tian Yuan[1,2], Weihao Wang[1,2], Huiyi Deng[1,2], Weifeng Kong[1,2], Jingyuan Chen[1,2], Yurong Bai[1,2], Yue Li[1], Yubin Chen[1,2], Qingwu Wu[1,2], Shuo Wu[1,2], Xuekun Huang[1,2], Zhaohui Shi[1,2], Qingling Fu[5,6], Yana Zhang[1,2,#], Qintai Yang[1,2,#]

Rhinology 62: 4, 0 - 0, 2024
https://doi.org/10.4193/Rhin23.520

Abstract

Background: Epithelial-mesenchymal transition (EMT) plays a crucial role in the pathogenesis of chronic rhinosinusitis with nasal polyps (CRSwNP). However, the involvement of small extracellular vesicles (sEVs) in EMT and their contributions to CRSwNP has not been extensively investigated. **Methods**: SEVs were isolated from nasal mucosa through ultracentrifugation. MicroRNA sequencing and reverse-transcription quantitative polymerase chain reaction were employed to analyze the differential expression of microRNAs carried by sEVs. Human nasal epithelial cells (hNECs) were used to assess the EMT-inducing effect of sEVs/microRNAs. EMT-associated markers were detected by western blotting and immunofluorescence. Dual-luciferase reporter assay was performed to determine the target gene of miR-375-3p. MicroRNA mimic, lentiviral, and plasmid transduction were used for functional experiments. **Results**: In line with the greater EMT status in eosinophilic CRSwNP (ENP), sEVs derived from ENP (ENP-sEVs) could induce EMT in hNECs. MiR-375-3p was elevated in ENP-sEVs compared to that in control and nonENP. MiR-375-3p carried by ENP-sEVs facilitated EMT by directly targeting KH domain containing RNA binding (QKI) at seed sequences of 913-919, 1025-1033, and 2438-2444 in 3'-untranslated region. Inhibition of QKI by miR-375-3p overexpression promoted EMT, which could be reversed by restoration of QKI. Furthermore, the abundance of miR-375-3p in sEVs was closely correlated with the clinical symptom score and disease severity. **Conclusions**: MiR-375-3p-enriched sEVs facilitated EMT by suppressing QKI in hNECs. The association of miR-375-3p with disease severity underscores its potential as both a diagnostic marker and a therapeutic target for the innovative management of CRSwNP.

Key words: nasal polyps, extracellular vesicles, microRNAs, epithelial-mesenchymal transition

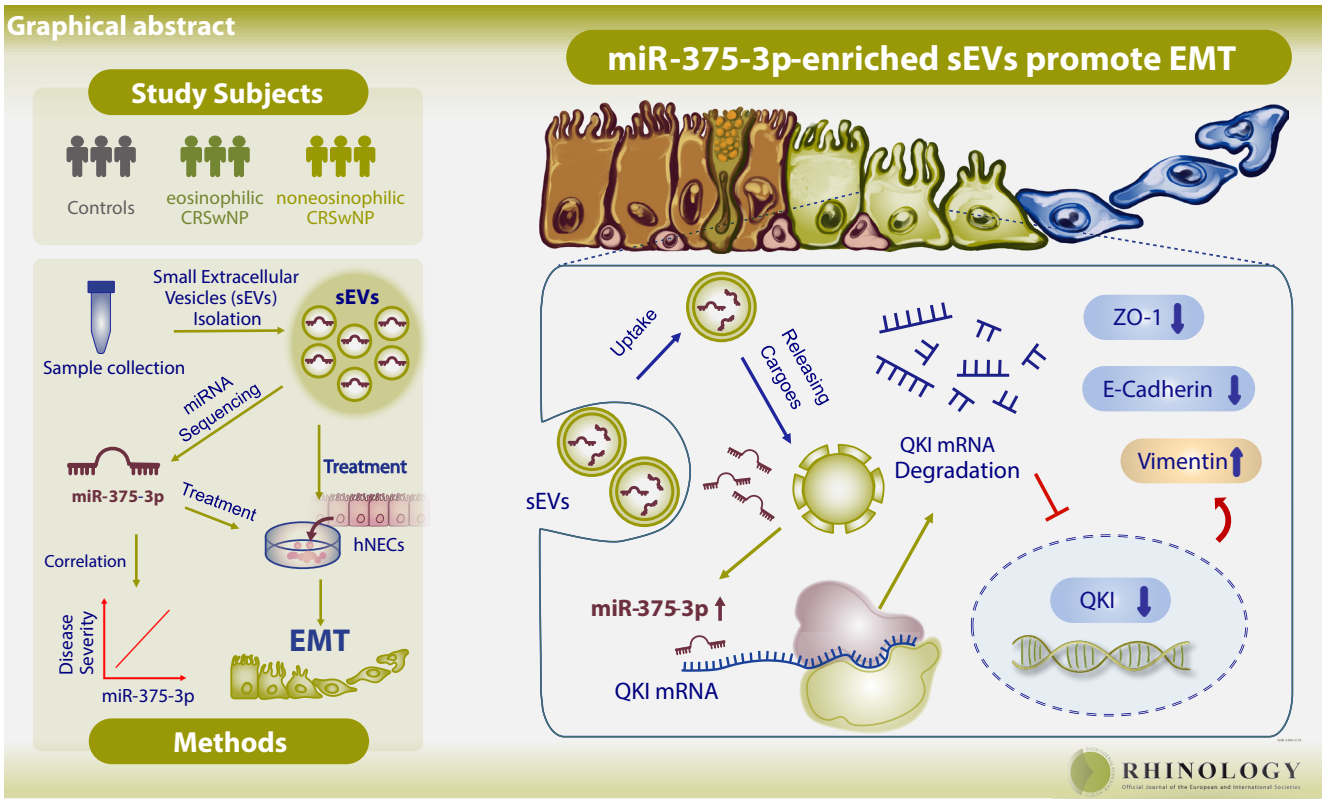

Introduction

Despite advances in medical and surgical therapy, chronic rhinosinusitis (CRS) remains associated with a high disease burden and is difficult to treat, particularly for patients with chronic rhinosinusitis with nasal polyps (CRSwNP). Eosinophilic inflammation has commonly been considered the predominant feature of CRSwNP [1], and usually leads to more severe symptoms and refractory [2]. The complex and heterogeneous nature of this disease poses a significant challenge for improving the treatment of eosinophilic CRSwNP (ENP).

Extracellular vesicles (EVs) are lipid-bilayer membrane structures that act as messengers, facilitating the horizontal transfer of nucleic acids, lipids, and proteins [3]. Despite the heterogeneity of their content, size, membrane components, and functions [3,4], EVs are generally divided into two subtypes based on their size: small EVs (sEVs, diameter <200 nm) and medium/large EVs (m/lEVs, diameter >200 nm) [3]. EVs influence various pathophysiological processes in multiple airway diseases, such as allergic rhinitis [5, 6], CRSwNP [7, 8], and asthma [9-11].

Epithelial-mesenchymal transition (EMT) is a biological process in which epithelial cells acquire mesenchymal characteristics and lose cell-cell interactions as well as apicobasal polarity. This process plays a crucial role in tissue remodeling and nasal polypogenesis [12]. Pioneering studies have demonstrated that EMT is augmented in ENP, correlating with eosinophil infiltration and disease severity [13-15]. Although accumulating evidence highlights on the key role of EVs, mainly sEVs extracted from cell culture supernatants/ body fluids, in EMT processes [7, 16, 17], it remains unclear whether EVs, especially those in the local microenvironment, can induce EMT and the underlying molecular mechanisms, especially in respiratory diseases, such as ENP.

In this study, we demonstrated the enrichment of sEVs in the nasal mucosa of patients with CRSwNP and reported that miR-375-3p-enriched sEVs contributed to EMT by inhibiting KH domain containing RNA binding (QKI) in CRSwNP.

Materials and methods

Subjects

This study was approved by the Ethics Committee of the Third Affiliated Hospital of Sun Yat-Sen University (File No. RG2023-124-01) and conducted with written informed consent from all participants. The diagnostic criteria of CRSwNP were according to the European Position Paper on Rhinosinusitis and Nasal Polyps 2020 [1]. Not all samples were included in every experiment protocol because of the limited quantity. The patients' characteristics are presented in Table S1.

Isolation of EVs

EVs from nasal mucosa were isolated using a protocol consisting of enzymatic treatment and differential ultracentrifugation as previously reported [18, 19].

Western blotting (WB)

WB was performed with corresponding antibodies (Supplemental Table S2 and S3).

Identification of EVs

The morphology of vesicles was examined via transmission electron microscopy (TEM). The size distribution of vesicles was evaluated using nanoparticle tracking analysis (NTA). The expression level of markers of EVs was measured by WB.

Reverse-transcription quantitative polymerase chain reaction (RT-qPCR)

Primers for mature miRNA assays were purchased from RiboBio (Guangzhou, China), others were listed in Supplemental Table S4. Differences in relative expression were calculated by the 2-ΔΔCt method.

MicroRNAs (miRNAs) sequencing and bioinformatics analysis

MiRNAs library construction and sequencing were performed by BGI Genomics (Shenzhen, China). According to the manufacturer's instructions, miRNAs were extracted from sEVs derived from 3 inferior turbinates (IT), 3 ENP, and 3 nonENP. MiRNA sequencing was performed on the DNBSEQ platform, and SOAPnuke was used to clean the tag. Differential expression analysis was performed with Bowtie2 (v2.2.5) software. All primary data have been uploaded to the Sequence Read Archive (NCBI) under the accession number PRJNA1023471.

Dual-luciferase reporter assay

Sequence analysis indicated that the 3' untranslated regions (UTR) of the QKI mRNA contains three conserved possible binding sites (913-919, 1025-1031, and 2438-2444) for miR-375-3p. Details of the reporter plasmids containing either wild-type (WT) or mutation (MT) versions of the 3'-UTR of QKI are listed in Supplemental Table S5. Different constructs were co-transfected with miR-375-3p mimic (RiboBio, China) into HEK 293T cells, respectively. According to the manufacturer's instructions, luciferase activity was measured 48 hours after transfection using the Dual-Luciferase Reporter Assay System (Promega, USA).

Human nasal epithelial cells (hNECs) culture

HNECs were isolated and cultured according to the method previously published [20].

Vector construction and transfection experiment

The human gene QKI and its mutants were cloned into Dual-Luciferase vectors, respectively. Lentiviral vectors carrying miR-375-3p inhibitor or QKI cDNA/shRNA were purchased from GeneCopoeia (Maryland, USA), while miRNA mimic was purchased from Ribobio (Guangzhou, China). More details are listed in Table S4.

SEVs uptake experiment

SEVs were labeled with PKH67 fluorescent dye (PKH67 fluorescent cell linker kit, Sigma, USA), then cocultured with hNECs. HNECs was labelled with Dil dye (1,1'-dioctadecyl-3,3,3',3'-tetramethylindocarbocyanine perchlorate, Invitrogen, USA). Images were acquired by fluorescence microscope (NIKON Ti2, Japan).

Immunofluorescence (IF) and immunohistochemistry (IHC)

IF and IHC were performed as previously reported[20]. Specific antibodies were listed in Table S2, S3.

Statistical analysis

GraphPad Prism version 8.0 (GraphPad Prism, La Jolla, CA, USA) software was used to analyze the data, which was expressed as median ± standard deviation or median and interquartile range. Differences between groups were analyzed using the Kruskal-Wallis analysis. Paired t-test analysis and one-way ANOVA analysis were used for in vitro data. Spearman analysis was used for correlation assessment. $P<0.05$ was considered significant. For microRNA sequencing analysis, differentially expressed miRNAs (DE-miRNAs) were regarded as significant while [log2 (Fold Change)]>1 as well as adjusted P value <0.05.

More detailed information about the methods used in the study is presented in the Supplementary Materials.

Results

ENP-sEVs promote EMT in hNECs

Both sEVs and m/lEVs are present in the nasal mucosa. The characteristics of EVs isolated from the nasal mucosa were analyzed. Both sEVs and m/lEVs exhibited typical bilayer membrane structures (Figure 1A). NTA results showed that the diameter of sEVs was smaller than 200nm, while that of m/lEVs was larger than 200nm (Figure 1B). WB analyses showed that both sEVs and m/lEVs highly expressed EV markers, including TSG101, CD9, and CD63, but scarcely expressed endoplasmic reticulum membrane marker Calnexin (Figure 1C). Additionally, results of protein quantification and particle count demonstrated that sEVs were more enriched in the nasal mucosal microenvironment than m/lEVs (Figures 1D and E).

Data from our team and others demonstrated augmented EMT in ENP compared with that in the nonENP and control group (Figure S1) [13, 15]. Since sEVs have been reported to be involved in physiological or pathological EMT progression in cancer [21-23], we hypothesized that sEVs might regulate EMT in the nasal mucosa. We found that sEVs could be taken up by hNECs, and started disintegrating and releasing the cargo upon internalization (Figure 1F). ENP-sEVs and nonENP-sEVs, but not IT-sEVs, downregulated the expression of Zonula occludens protein 1 (ZO-1) and E-Cadherin. However, compared to nonENP-sEVs and IT-sEVs, only ENP-sEVs steadily upregulated Vimentin expression in hNECs (Figure 1G), demonstrating that ENP-sEVs, but not nonENP-sEVs, facilitated EMT in hNECs. Furthermore, morphological analysis showed that hNECs transformed into a slender shape after treatment with ENP-sEVs, implying a transition from epithelial to mesenchymal cells (Figure 1H). IF staining showed the decreased expression of ZO-1 and E-Cadherin and increased expression of Vimentin in ENP-sEVs-treated hNECs (Figure 1I). These results suggest that ENP-sEVs facilitate EMT progression in hNECs.

MiR-375-3p is overexpressed in ENP-sEVs

We investigated the mechanisms by which ENP-sEVs contribute to EMT progression. While sEVs primarily deliver nucleic acids, proteins, and metabolites to recipient cells, miRNAs constitute their major components of EVs [24]. Moreover, miRNAs are known to regulate EMT and participate in polypogenesis in CRS [25-28]. Hence, we sequenced the miRNA expression profiles of sEVs from ENP, nonENP, and control samples. Principal component analysis (PCA) revealed distinct partitioning of sEVs among the three groups (Figure 2A). The DE-miRNAs in the sEVs are depicted in a heat map according to the reads per million mapped reads and the fold change (Figure 2B and Table S6). In total, there were 14 upregulated and 12 downregulated miRNAs within ENP-sEVs compared to IT-sEVs. Additionally, two upregulated miRNAs and one downregulated miRNA were identified in nonENP-sEVs compared with IT-sEVs. Only one miRNA was upregulated in nonENP-sEVs compared to ENP-sEVs (Figure 2B and Table S6). Among all the DE-miRNAs, miR-375-3p exhibited the highest expression level in sEVs (Figures 2C and D). Since miR-375-3p plays a crucial role in regulating EMT progression in cancer [29, 30], we hypothesized that miR-375-3p may affect EMT events in hNECs. Therefore, ENP-sEVs-derived miR-375-3p was chosen for further functional studies. RT-qPCR further confirmed that miR-375-3p was significantly increased in ENP-sEVs compared with that in both nonENP-sEVs and IT-sEVs (Figure 2E). These findings indicated that the enriched miR-375-3p derived from ENP-sEVs may contribute to EMT progression of ENP.

MiR-375-3p facilitates EMT in hNECs

We aimed to clarify whether miR-375-3p regulates EMT in hNECs. RT-qPCR revealed an elevated expression level of miR-375-3p in hNECs treated with ENP-sEVs (Figure 3A). As anticipated, miR-375-3p mimic recapitulated the phenotype induced by ENP-sEVs. Firstly, histomorphological studies showed morphological characteristics with slender shape transformation and missing apicobasal polarity in hNECs after administration of miR-375-3p mimic for 72h (Figure 3B). Next, IF results demonstrated decreased expression levels of epithelial markers such as E-Cadherin and ZO-1, along with increased expression of the mesenchymal marker Vimentin in hNECs infected with miR-375-3p mimic (Figure 3C). Consistent with IF, WB results further

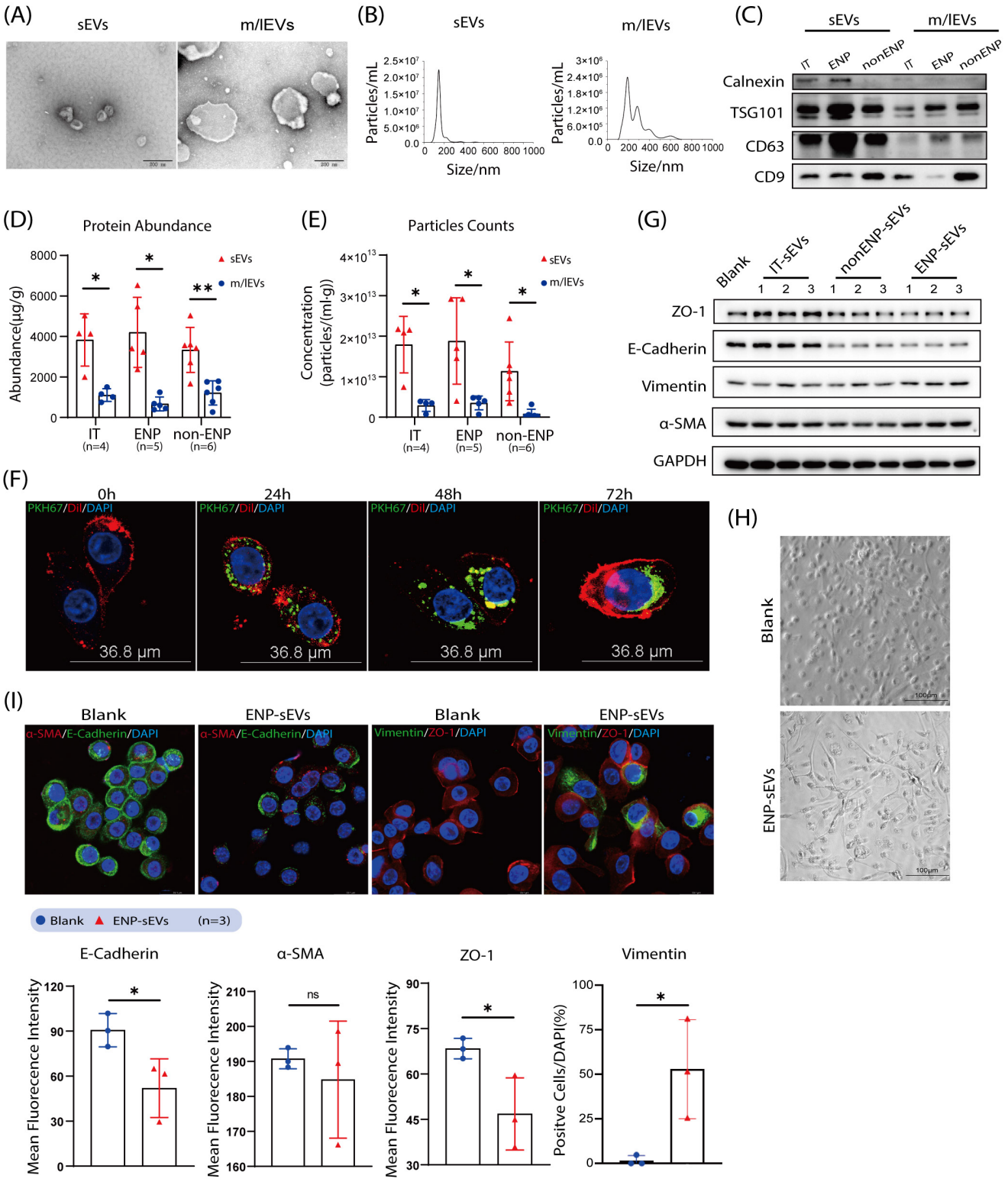

Figure 1. ENP-sEVs promote EMT in hNECs. A) Representative photomicrographs of sEVs and m/IEVs observed by transmission electron microscopy. Scale bar, 200nm. B) Representative graphs showing the particle size distribution of sEVs and m/IEVs measured by NTA. C) WB analysis of markers (CD9, CD63, and TSG101) and internal protein marker (Calnexin) for EVs. D) and E) Quantitative analyses of sEVs and m/IEVs by NTA and WB, respectively. F) Representative photomicrographs showing the uptake of sEVs labeled with PKH67 (green) by hNECs for 0h, 24h, 48h and 72h in vitro (×630 magnification). Scale bar, 36.8μm. G) WB analysis of ZO-1, E-Cadherin, Vimentin and α-SMA protein expression in hNECs treated with sEVs (15μg) isolated from control, ENP, and nonENP subjects for 72h. H) Representative phase contrast images showing morphological features of EMT in hNECs treated with ENP-sEVs (15μg) for 72h (×400 magnification). Scale bar, 10μm. I) Representative IF images and quantitative analysis of EMT biomarkers including ZO-1, E-Cadherin, Vimentin and α-SMA in hNECs (×630 magnification). Scale bar, 23.1μm. *P<0.05, **P<0.01.

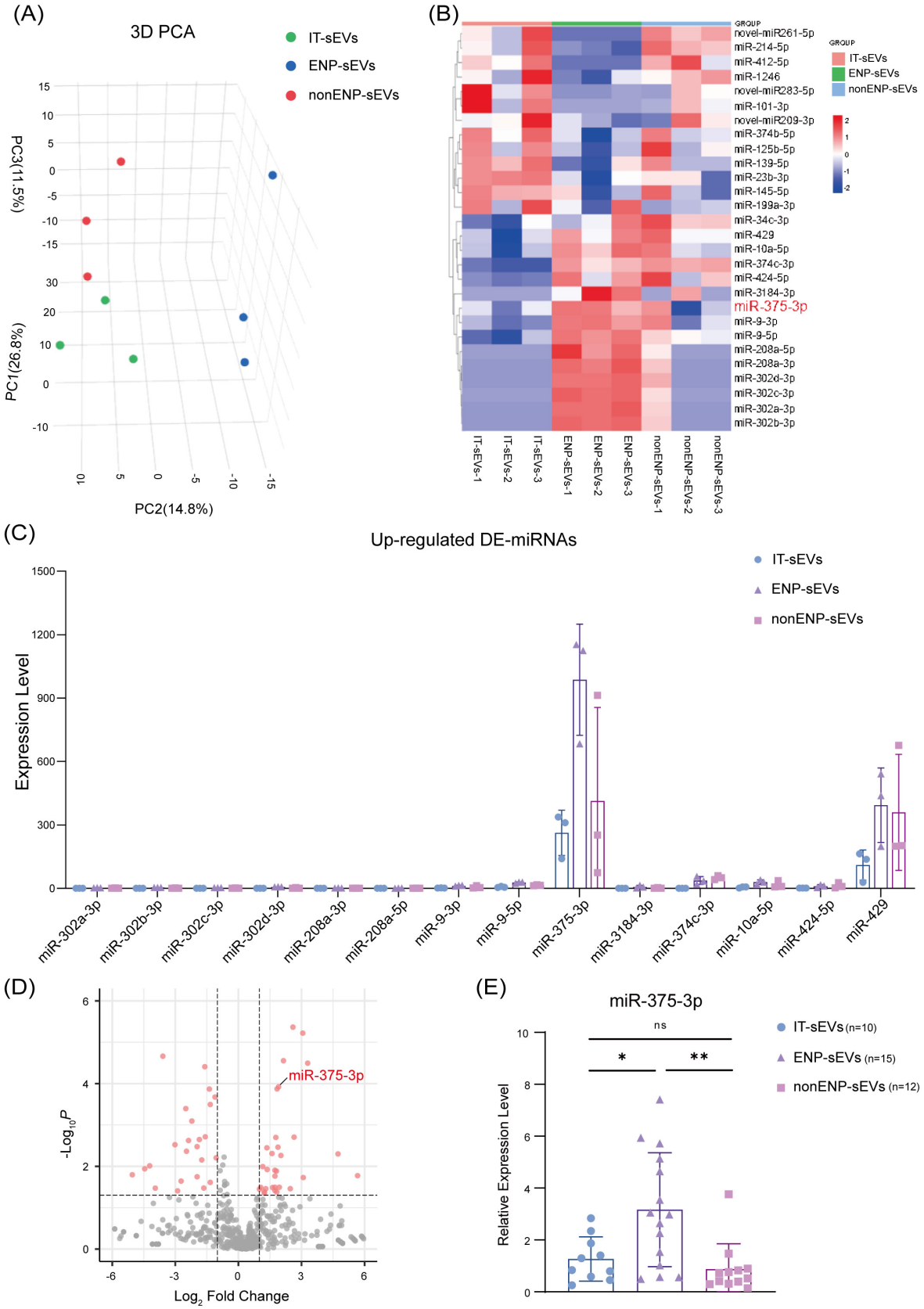

Figure 2. MiR-375-3p is overexpressed in ENP-sEVs. A) Principal component analysis plots for miRNA seq data from sEVs. B) Heatmap showing the relative abundance of DE-miRNAs in sEVs derived from control, ENP, and nonENP individuals. C) Relative levels of upregulated miRNAs from sEVs among the three groups. D) The volcano plot showing DE-miRNAs between ENP-sEVs and IT-sEVs. E) Relative expression level of miR-375-3p in sEVs isolated from the three studied groups. *P<0.05; **P<0.01.

confirmed that miR-375-3p mimic mediated EMT in hNECs, as indicated by the upregulated protein expression level of Vimentin, and downregulated protein levels of E-Cadherin and ZO-1 in hNECs transfected with miR-375-3p mimic (Figure 3D). Due to the limited inhibitory efficacy of the commercial miR-375-3p inhibitor, a concentrated viral solution containing the miR-375-3p inhibitor (HmiR-375-3p) clone was used to infect hNECs. In contrast, transfection with HmiR-375-3p could counteract the EMT induced by miR-375-3p mimic in hNECs ex vivo (Figure 3E).

MiR-375-3p directly targets QKI

To predict the target genes of miR-375-3p in hNECs, publicly available algorithms including miRDB, Tarbase, and Targetscan were used. A total of 33 shared targets were identified, with the top 10 genes selected for further confirmation (Figure 4A and Table S7). Relative mRNA expression levels of these putative target genes were assessed in miR-375-3p overexpressed hNECs. As shown in Figure 4B, while both QKI and Kruppel-like factor transcription factor 5 (KLF5) were repressed following miR-375-3p overexpression, QKI exhibited the most pronounced inhibition. More importantly, QKI has been described to inhibit EMT in carcinoma [31]. In contrast to miR-375-3p, we confirmed that the mRNA expression level of QKI was downregulated in ENP compared to that in IT and nonENP (Figure 4C). Therefore, we hypothesized that QKI is a critical target gene of miR-375-3p in hNECs. The binding sites of QKI mRNA were analyzed to test for direct binding between miR-375-3p and QKI. Sequence analysis indicated that the 3′-UTR of QKI mRNA contains three conserved possible binding sites (913-919, 1025-1031, and 2438-2444) for miR-375-3p (Figure 4D). Three predicted binding sites were cloned and inserted into the luciferase reporter vector (pmiRGLO). Wild type (WT) 1+2 contained binding sites 913-919 and 1025-1031, while WT3 contained binding sites 2438-2444. Consequently, four mutated types (MT1 with mutations at site 913-919, MT2 with mutations at site 1025-1033, MT1+2 contained double mutations at sites 913-919, and 1025-1031, MT3 with mutations at site 2438-2444). Subsequently, a Dual-luciferase reporter assay was performed to determine the relative luciferase activity under the condition of miR-375-3p mimic treatment in HEK 293T cells transfected with QKI 3′-UTR WT or QKI 3′-UTR MT reporter plasmids. As shown in Figure 4E, reduced relative luciferase activity was observed when QKI 3′-UTR WT1+2 or WT3 was co-transfected with miR-375-3p mimic. Furthermore, the relative luciferase activity decreased after co-transfection of miR-375-3p with QKI 3′-UTR MT1 or with MT2, but not with MT1+2 or with MT3 (Figure 4E). These findings suggested that miR-375-3p targets QKI by binding to the seed sequences of 913-919, 1025-1033, and 2438-2444 in 3′-UTR.

MiR-375-3p derived from ENP-sEVs downregulates the expression of QKI in hNECs

To test whether miR-375-3p carried by ENP-sEVs could regulate QKI in hNECs, ENP-sEVs were administrated to hNECs, and significant downregulation of QKI mRNA expression level was observed after 72h of treatment (Figure 5A). IF staining indicated a decreased proportion of QKI-positive cells in hNECs treated with ENP-sEVs (Figure 5B). WB also evidenced the downregulation of QKI protein expression in hNECs treated with ENP-sEVs (Figure 5C). To further confirm the relationship between miR-375-3p and QKI, hNECs were stimulated with miR-375-3p mimic to observe both mRNA and protein expression levels of QKI. As expected, miR-375-3p mimic treatment efficiently inhibited the mRNA level of QKI in hNECs (Figure 5D). Consistent with the decreased QKI mRNA level, IF results showed that overexpression of miR-375-3p in hNECs significantly reduced the proportion of QKI-positive cells (Figure 5E). WB further confirmed that the QKI protein level was significantly decreased when hNECs were treated with miR-375-3p mimic (Figure 5F). HNECs transfected with HmiR-375-3p demonstrated upregulated QKI mRNA and protein levels (Figures 5G and H). These data strongly imply that QKI is a target of miR-375-3p in hNECs.

MiR-375-3p regulates EMT progress through QKI in hNECs

We investigate whether miR-375-3p regulates EMT by targeting QKI in hNECs. To test this hypothesis, lentivirus carrying QKI shRNA and lentivirus carrying QKI cDNA were transfected into hNECs, respectively. As expected, both mRNA and protein levels of QKI were efficiently blunted in hNECs transfected with lentivirus carrying QKI shRNA (Figures 6A and B). WB demonstrated that the expression levels of Vimentin was upregulated, whereas those of E-Cadherin and ZO-1 were downregulated in hNECs transfected with lentivirus carrying QKI shRNA (Figure 6C). In contrast, overexpression of QKI in hNECs with lentivirus carrying QKI cDNA (Figures 6D and E) displayed elevated E-Cadherin and ZO-1 expression and downregulated Vimentin expression (Figure 6F). These results suggest that QKI plays an important role in blocking EMT progression. Furthermore, we aimed to determine whether miR-375-3p promotes EMT progression by inhibiting QKI expression in hNECs. HNECs were first transferred with miR-375-3p mimic, then co-transferred with lentivirus carrying QKI cDNA. Both mRNA and protein levels of repressed QKI could efficiently be re-upregulated by QKI overexpression in lentivirus-infected hNECs (Figures 6G and H). Consistent with the QKI expression level, miR-375-3p mimic transfection rescued the protein level of Vimentin but inhibited E-Cadherin and ZO-1 expression induced by QKI overexpression in hNECs (Figure 6I). These data imply that miR-375-3p promotes EMT by blunting QKI expression in hNECs.

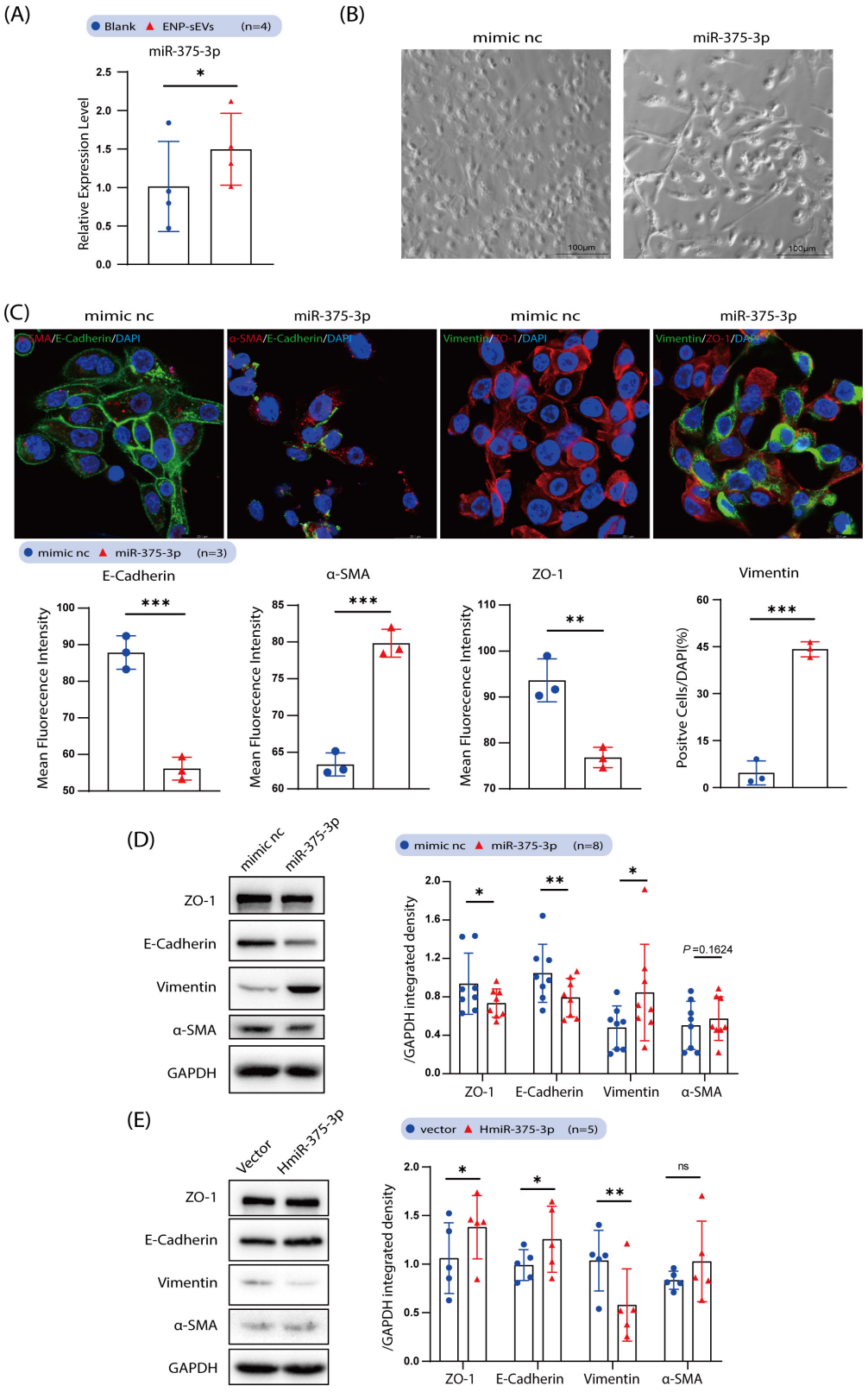

Figure 3. MiR-375-3p facilitates EMT in hNECs. A) Relative expression level of miR-375-3p in hNECs treated with ENP-sEVs (15μg) for 72h. B) Representative phase contrast images of hNECs treated with miR-375-3p mimic for 72h (×400 magnification). Scale bar, 10μm. C) Representative IF photomicrographs and quantitative analysis of EMT associated biomarkers including ZO-1, E-Cadherin, Vimentin and α-SMA in hNECs administrated with miR-375-3p mimic and mimic nc (×630 magnification). Scale bar, 23.1μm. D) HNECs were treated with miR-375-3p mimic and mimic nc for 72h. The indicated proteins were immunoblotted in lysates from the hNECs. E) HNECs were infected with lentivirus carrying miR-375-3p inhibitor (HmiR-375-3p) or control lentivirus (vector) for 72h. The EMT-associated proteins were immunoblotted. *P<0.05; **P<0.01; ***P<0.001.

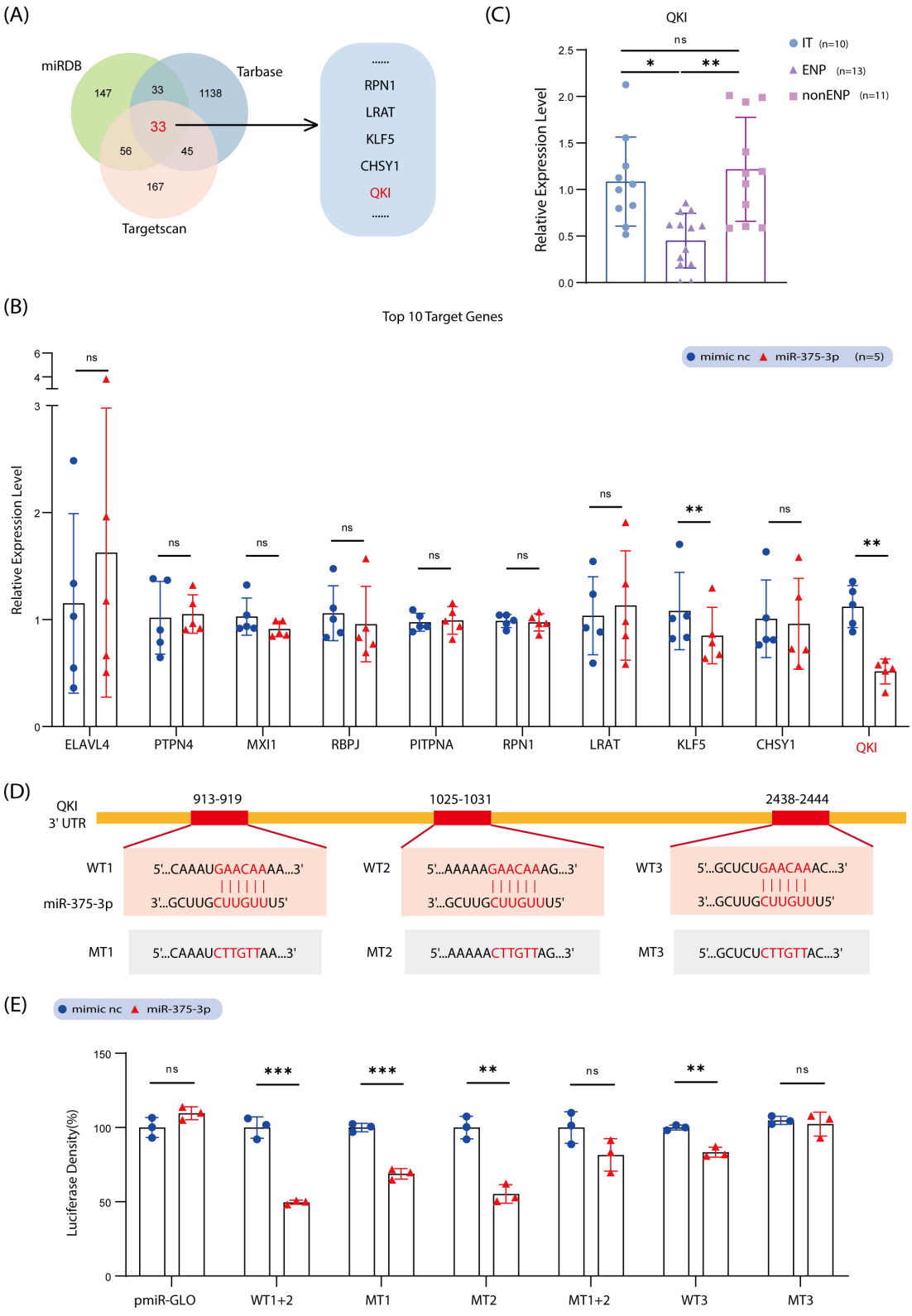

Figure 4. MiR-375-3p directly targets QKI. A) Venn diagram showing putative miR-375-3p targets screened using miRDB, TargetScan and Tarbase database. B) Relative expression level of the top ten target genes in hNECs treated with miR-375-3p mimic for 48h. C) Relative expression level of QKI mRNA in nasal mucosa tissue from different groups. D) TargetScan predicted the 3'-UTR of QKI mRNA contains 3 possible binding sites (913-919, 1025-1031, and 2438-2444) for miR-375-3p. Homologous analysis of the binding sequence among indicated sequences of mutated human 3'-UTR of QKI mRNA. E) Association between miR-375-3p and QKI was indicated by luciferase reporter assay. Plasmids of luciferase reporter construction containing the wild-type 3'-UTR of QKI mRNA (WT1+2, WT3) and mutated 3'-UTR of QKI mRNA (MT1, MT2, MT1+2, MT3) were generated, and were co-transfected with miR-375-3p mimic in HEK 293 T cells for 48h. *P<0.05; **P<0.01; ***P<0.001.

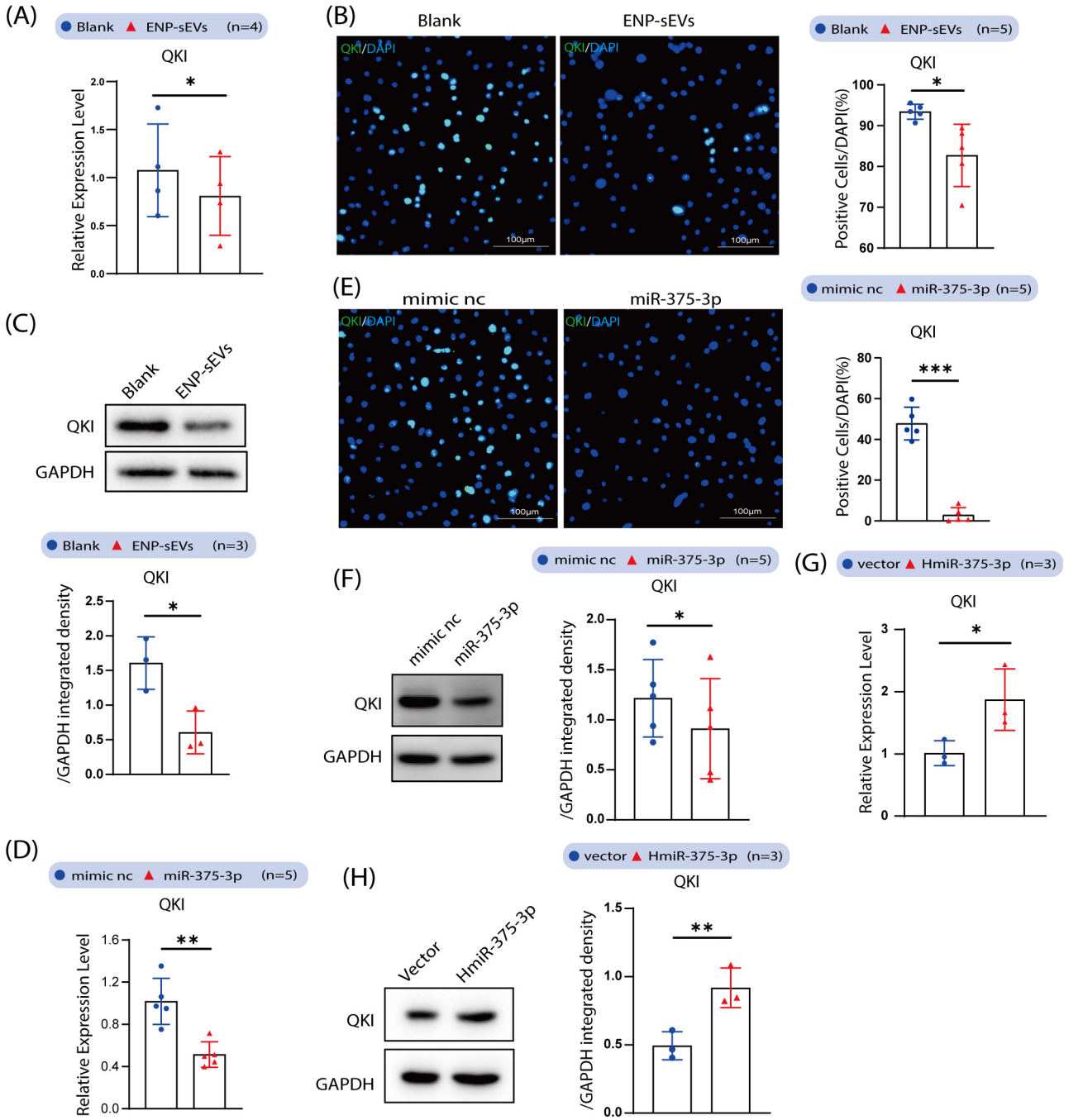

Figure 5. MiR-375-3p carried by ENP-sEVs represses the expression of QKI in hNECs. A) Relative expression level of QKI mRNA in hNECs treated with ENP-sEVs for 72h. B) Representative IF photomicrographs and quantitative analysis of QKI in hNECs treated with ENP-sEVs for 72h (×400 magnification). Scale bar, 10μm. C) Representative blots of QKI in lysates from hNECs treated with ENP-sEVs for 72h. D) QKI mRNA expression level in hNECs treated with miR-375-3p mimic for 72h. E) Representative IF photomicrographs and quantitative analysis of QKI in hNECs treated with miR-375-3p for 72h (×400 magnification). Scale bar, 10μm. F) Representative blots of QKI in lysates from hNECs treated with miR-375-3p and mimic nc for 72h. G) Relative mRNA and expression level of QKI in hNECs infected with lentivirus carrying miR-375-3p inhibitor (HmiR-375-3p) for 72h. H) Representative blots of QKI in lysates from hNECs treated with lentivirus carrying miR-375-3p inhibitor (HmiR-375-3p) for 72h. *P<0.05; **P<0.01; ***P<0.001.

MiR-375-3p carried by sEVs correlates to CRSwNP severity

We analyzed the relationship between miR-375-3p and clinical parameter scores of patients with CRSwNP. We discovered that the expression level of miR-375-3p was positively correlated with the SinoNasal Outcomes Test 22 (SNOT22) score, Visual Analogue Scale (VAS) score, and Lund-Mackay Computed Tomography (CT) score (Supplemental Figure S2, A-C), suggesting that the miR-375-3p level derived from NP-sEVs was tightly associated with the severity of CRSwNP. Additionally, the miR-375-3p level was positively related to olfactory score from

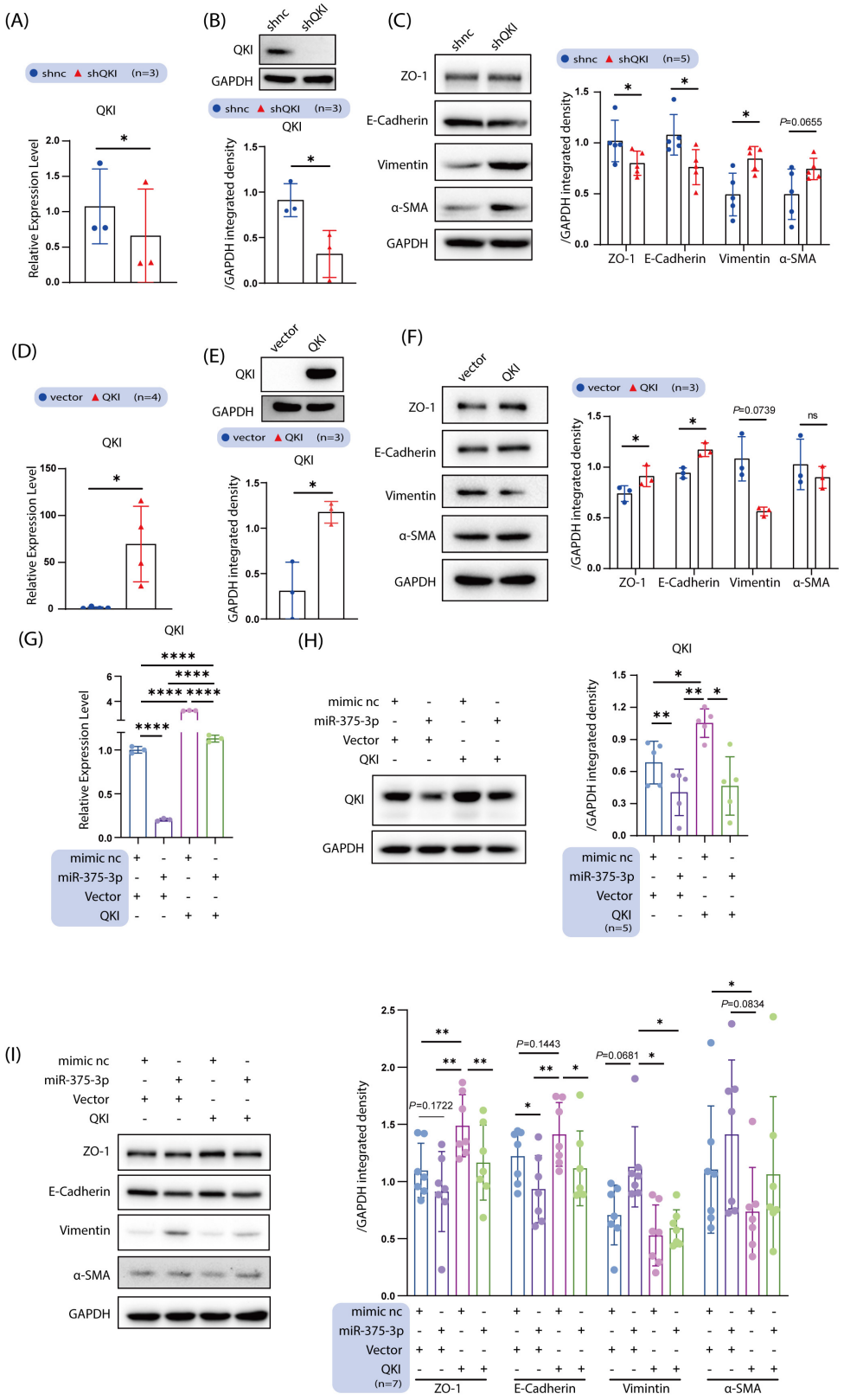

Figure 6. MiR-375-3p regulates EMT progress through QKI repression in hNECs. A) Relative mRNA and B) protein expression level of QKI in hNECs transduced with shQKI lentivirus or shControl lentivirus (shnc) for 72h. C) Representative blots of EMT biomarkers in lysates from hNECs treated with shQKI for 72h. D) Relative mRNA and E) protein expression level of QKI in hNECs transduced with lentivirus carrying QKI cDNA (QKI) or empty vector in hNECs for 72h. F) Representative blots of EMT biomarkers in lysates from hNECs treated with QKI for 72h. G-I) HNECs were treated with miR-375-3p mimic for 48h, followed by QKI overexpression for 48h. G) Relative mRNA and H) protein expression level of QKI in hNECs. I) Protein expression level of EMT-associated biomarkers including ZO-1, E-Cadherin, Vimentin and α-SMA in hNECs. *P<0.05; **P<0.01; ****P<0.0001.

VAS, Questionnaire of Olfactory Disorders Negative Statements (QOD-NS), and Threshold Discrimination Identification (TDI) score (Supplemental Figure S2, D-F), as well as the percentage of tissue eosinophils (Supplemental Figure S2, G), implying that miR-375-3p may contribute to olfactory disorder and eosinophil infiltration. Thus, miR-375-3p obtained in NP-sEVs may serve as a new biomarker for evaluating disease severity and olfactory function.

Discussion

Evidence has demonstrated that the involvement of polypogenesis in EMT processes [12-15]. However, the underlying molecular mechanisms of this involement remain unclear. In this study, we found that sEVs derived from ENP milieu promoted EMT in hNECs, which may contribute to hyperplasia and subsequent polyposis. Mechanistically, ENP-sEVs facilitated EMT by delivering the miR-375-3p cargo, which directly targeted and repressed QKI in hNECs. Based on these findings, we proposed that miR-375-3p-enriched sEVs might underlie polypogenesis by inhibiting QKI expression. Moreover, miR-375-3p in sEVs may be positively associated with disease severity; further, it is a potential therapeutic target against CRSwNP.

While EVs obtained from nasal lavage fluids, cell culture supernatants, plasma, and microbiota have been reported to be associated with the pathogenesis of CRSwNP [16, 32-35], they are limited by their inability to accurately reflect the pathophysiological characteristics and three-dimensional structure of tissues [4]. This study provided evidence of the presence and accumulation of sEVs in the nasal mucosa, suggesting that sEVs might play a critical role in the pathophysiology of CRSwNP. Similar to characteristics of EVs derived from body fluid and cell supernatants, both sEVs and m/lEVs derived in nasal tissues displayed a typical "tea-cup" shape, with high expression levels of EVs markers such as TSG101, CD9, and CD63. We did not observe an elevated abundance or concentration of EVs derived from CRSwNP compared to the control group. This was consistent with the results from mucus-derived EVs [36]. However, EVs isolated from nasal lavage fluid are increased in CRSwNP [8, 37]. The discrepancy may arise from distinct sources and different subtypes of EVs from supernatants/body fluid versus tissue microenvironments. Furthermore, the current study presents compelling evidence that miR-375-3p-enriched sEVs facilitate the EMT process, as indicated by the decreased expression of epithelial biomarkers (ZO-1 and E-Cadherin), and increased expression of the mesenchymal marker, Vimentin in ENP-sEVs/miR-375-3p treated hNECs. Previous studies have indicated that EMT events are more prominent in ENP than in nonENP [13-15], implying that ENP-sEVs, at least partially, exert a pivotal function in driving EMT.

Various studies have corroborated the contribution of sEVs to EMT, with miRNAs garnering substantial attention for their role in sEVs in tumor cells. For example, Liang et al. [23] reported that miR-let-7c-rich sEVs from oral squamous cell carcinoma promote EMT via the p53/PTEN pathway, whereas miR-19b-3p within sEVs from cancer stem cells induce EMT by repressing PTEN [38]. Hypoxia also participates in sEV-mediated EMT, and sEVs derived from hypoxia-preconditioned mesenchymal stem cells increase proliferation and EMT of non-small cell lung cancer cells by delivering miR-21-5p [39]. Beyond the function of sEVs on EMT in cancer, miR-21-5p in sEVs released by rat alveolar macrophages promoted EMT in tracheal epithelial cells via the TGFβ1/SMAD7 pathway under stress conditions [28]. Few studies have confirmed that miRNAs carried by sEVs are involved in EMT in human upper airway diseases, especially CRSwNP. Since sEVs exert their biological functions by delivering miRNAs to recipient cells to induce EMT, we conducted miRNA sequencing of sEVs isolated from different nasal mucosa sources.

Beyond to our novel finding of miR-375-3p, several miRNAs, such as miR-155-3p [27], miR-200a-3p [25], miR-761 [26], miR-21 [28], and miR-182 [15] have been reported to be involved in EMT in CRS. However, the expression levels of these miRNAs in sEVs were low, therefore, we focused on how miR-375-3p regulates EMT. Our results demonstrated that elevated miR-375-3p "messages" delivered by ENP-sEVs could effectively be perceived and captured by hNECs. Subsequently, this led to decreased epithelial markers (ZO-1 and E-Cadherin) and increased mesenchymal marker (Vimentin) expression in hNECs. These findings strongly suggest that miR-375-3p is a pivotal cargo in ENP-sEVs and facilitates EMT in ENP. Currently, the expression pattern and contribution of miR-375-3p to airway inflammatory diseases remain controversial. Some researchers have observed the downregulation expression of miR-375 in patients with asthma and/or AR, as well as its anti-inflammatory function [40, 41]. However, conflicting results demonstrated upregulated expression of miR-375 in airway inflammatory diseases. Bertram et al. [42] reported miR-375 upregulation in human bronchial cells following exposure to diesel exhaust particles and ambient particulate matter exposure. Elevated miR-375 expression has also been noted in smokers with COPD [43], childhood asthma [44], and AR [45]. Moreover, the function of miR-375-3p in EMT events remains unclear; it was implicated as an EMT inducer in prostate cancer [29], but was deemed as an EMT inhibitor in colon cancer [46] and hepatocellular carcinoma [47]. These conflicting results suggest that miR-375 has different functions in distinct tissue environments and disease statuses.

Furthermore, employing bioinformatic and quantitative analyses, we demonstrated the seed sequences of 913-919, 1025-1031, and 2438-2444 in the 3'-UTR of QKI mRNA were the targeting sites of miR-375-3p. We further found that miR-375-3p overexpression promoted EMT by inhibiting QKI expression in hNECs. This observation is justified by previous research indicating the role of QKI in repressing EMT in lung cancer [31, 48] as well as facilitating EMT in hepatocellular carcinoma and pancreatic

cancer [49, 50]. In contrast, QKI overexpression using lentivirus-mediated transfection counteracted miR-375-3p-mediated EMT in hNECs ex vivo. These results imply that miR-375-3p promotes EMT by repressing the QKI gene in inflammatory upper airway diseases, such as CRSwNP, thus indicating that deactivating miR-375-3p may be a promising therapeutic target for CRSwNP.

Our study has some limitations. Firstly, since both sEVs and miR-375-3p could drive EMT, in addition to sEVs, miR-375-3p in eosinophilic nasal polyps may also correlate with disease severity, which should be studied in the future. Secondly, a variety of mixed miRNAs are carried by sEVs, and despite their low abundance, some of these miRNAs may play important roles. The functions of other miRNAs involved in EMT should be elucidated in future studies. Thirdly, proteins are also essential cargo within EVs, and proteins from sEVs may contribute to EMT. Thus, a comprehensive analysis of protein components in sEVs would enhance our understanding of EMT mechanisms in CRSwNP.

Conclusion

This study offers a direct insight into sEVs within the inflammatory environment of the nasal mucosa. Our findings uncovered a novel sEVs-mediated EMT mechanism in the inflammatory microenvironment of CRSwNP, driven by the miR-375-3p/QKI pathway. This study highlights the potential of sEVs in both fundamental research and clinical applications related to CRSwNP.

Acknowledgements

The authors thank Dr. Xu-Yun Peng from the University of Sun Yat-Sen for experimental technique help.

Authorship contribution

XW and RZ performed sEVs isolation, cell culture, bioenergetic analysis, immunological staining and data discussion. WL performed the lentiviral vector construction. TY, WW and HD performed cell culture and PCR assay. WK, YL, WW, YC, SW, XH and ZS participated in epithelial cell sample collection. JC, YB and HQ participated in clinical information collection. YZ and QY designed the study and prepare the manuscript. YZ, QY and QF, proofread the manuscript. All authors reviewed the manuscript.

Conflict of interest

The authors have no competing interests to declare.

Funding

This study was supported by the National Key R&D Program of China 2022YFC250410 (Q.Y.), the National Natural Science Foundation of China (NSFC) grants 82271148 and U20A20399 (Q.Y.), 82171114 and 82371121 (Y.Z.), 82000958 (R.Z.), 82271191 (Q.W.), 82101197 (T.Y.), the Key-area Research and Development Program of Guangdong Province 2020B0101130015 (Q.Y.), Guangdong Basic and Applied Basic Research Foundation 2021A1515011764 (Q.Y.), Young Talent Support Project of Guangzhou Association for Science and Technology, Science and Technology Program of Guangzhou, China 2023A04J1093 and QT20220101319 (R.Z.), and Sun Yat-sen University Clinical Research 5010 Program 2019006 (Q.Y.).

References

1. Fokkens W J, Lund V J, Hopkins C, et al. European Position Paper on Rhinosinusitis and Nasal Polyps 2020. Rhinology, 2020,58(Suppl S29):1-464.
2. Tokunaga T, Sakashita M, Haruna T, et al. Novel scoring system and algorithm for classifying chronic rhinosinusitis: the JESREC Study. Allergy. 2015 Aug;70(8):995-1003.
3. Thery C, Witwer K W, Aikawa E, et al. Minimal information for studies of extracellular vesicles 2018 (MISEV2018): a position statement of the International Society for Extracellular Vesicles and update of the MISEV2014 guidelines. J Extracell Vesicles, 2018,7(1):1535750.
4. Li S R, Man Q W, Gao X, et al. Tissue-derived extracellular vesicles in cancers and non-cancer diseases: Present and future. J Extracell Vesicles, 2021,10(14):e12175.
5. Fang S B, Zhou Z R, Peng Y Q, et al. Plasma EVs display antigen-presenting characteristics in patients with allergic rhinitis and promote differentiation of Th2 cells. Front Immunol, 2021,12:710372.
6. Zhu X, Sun Y, Yu Q, Wang X, Wang Y, Zhao Y. Exosomal lncRNA GAS5 promotes M1 macrophage polarization in allergic rhinitis via restraining mTORC1/ULK1/ATG13-mediated autophagy and subsequently activating NF-κB signaling. Int Immunopharmacol. 2023 Aug;121:110450.
7. Wang L F, Lee C H, Liang S S, et al. Mucin 5AC is significantly upregulated in exosomes from the nasal lavage fluid and may promote the expression of COX-2, VEGF and MMP-9: an implication in nasal polyp pathogenesis. Rhinology, 2021,59(3):328-336.
8. Takahashi T, Kato A, Berdnikovs S, et al. Microparticles in nasal lavage fluids in chronic rhinosinusitis: Potential biomarkers for diagnosis of aspirin-exacerbated respiratory disease. J Allergy Clin Immunol, 2017,140(3):720-729.
9. Brandsma J, Schofield J, Yang X, et al. Stratification of asthma by lipidomic profiling of induced sputum supernatant. J Allergy Clin Immunol, 2023,152(1):117-125.
10. Kulshreshtha A, Ahmad T, Agrawal A, Ghosh B. Proinflammatory role of epithelial cell-derived exosomes in allergic airway inflammation. J Allergy Clin Immunol. 2013 Apr;131(4):1194-203, 1203.e1-14.
11. Shin T S, Kim J H, Kim Y S, et al. Extracellular vesicles are key intercellular mediators in the development of immune dysfunction to allergens in the airways. Allergy, 2010,65(10):1256-1265.
12. Lee M, Kim D W, Yoon H, et al. Sirtuin 1 attenuates nasal polypogenesis by suppressing epithelial-to-mesenchymal transition. J Allergy Clin Immunol, 2016,137(1):87-98.
13. Yan B, Wang Y, Li Y, Wang C, Zhang L. Inhibition of arachidonate 15-lipoxygenase reduces the epithelial-mesenchymal transition in eosinophilic chronic rhinosinusitis with nasal polyps. Int Forum Allergy Rhinol. 2019 Mar;9(3):270-280.
14. Wang M, Sun Y, Li C, Qu J, Zhou B. Eosinophils correlate with epithelial-mesenchymal transition in chronic rhinosinusitis with nasal polyps. ORL J Otorhinolaryngol Relat Spec. 2022;84(1):70-80.
15. Jiang W, Zhou C, Ma C, Cao Y, Hu G, Li H. TGF-β1 induces epithelial-to-mesenchymal transition in chronic rhinosinusitis with nasal polyps through microRNA-182. Asian Pac J Allergy Immunol. 2021 Dec 26.
16. Takahashi T, Schleimer RP. Epithelial-cell-derived extracellular vesicles in pathophysiology of epithelial injury and repair in chronic rhinosinusitis: connecting immu-

nology in research lab to biomarkers in clinics. Int J Mol Sci. 2021 Oct 28;22(21):11709.
17. Song Q, Yu H, Cheng Y, et al. Bladder cancer-derived exosomal KRT6B promotes invasion and metastasis by inducing EMT and regulating the immune microenvironment. J Transl Med, 2022,20(1):308.
18. Crescitelli R, Lasser C, Jang S C, et al. Subpopulations of extracellular vesicles from human metastatic melanoma tissue identified by quantitative proteomics after optimized isolation. J Extracell Vesicles, 2020,9(1):1722433.
19. Kowal J, Arras G, Colombo M, et al. Proteomic comparison defines novel markers to characterize heterogeneous populations of extracellular vesicle subtypes. Proc Natl Acad Sci U S A, 2016,113(8):E968-E977.
20. Li Y, Chang L H, Huang W Q, et al. IL-17A mediates pyroptosis via the ERK pathway and contributes to steroid resistance in CRSwNP. J Allergy Clin Immunol, 2022,150(2):337-351.
21. Wang T, Wang X, Wang H, et al. High TSPAN8 expression in epithelial cancer cell-derived small extracellular vesicles promote confined diffusion and pronounced uptake. J Extracell Vesicles, 2021,10(13):e12167.
22. Liu X, Li J, Yang X, et al. Carcinoma-associated fibroblast-derived lysyl oxidase-rich extracellular vesicles mediate collagen crosslinking and promote epithelial-mesenchymal transition via p-FAK/p-paxillin/YAP signaling. Int J Oral Sci, 2023,15(1):32.
23. Liang W, Chen Y, Liu H, et al. Cancer cells corrupt normal epithelial cells through miR-let-7c-rich small extracellular vesicle-mediated downregulation of p53/PTEN. Int J Oral Sci, 2022,14(1):36.
24. Zhang X, Liu D, Gao Y, et al. The biology and function of extracellular vesicles in cancer development. Front Cell Dev Biol, 2021,9:777441.
25. Wu Y, Sun K, Tu Y, et al. miR-200a-3p regulates epithelial-mesenchymal transition and inflammation in chronic rhinosinusitis with nasal polyps by targeting ZEB1 via ERK/p38 pathway. Int Forum Allergy Rhinol, 2024 Jan;14(1):41-56.
26. Cheng J, Chen J, Zhao Y, Yang J, Xue K, Wang Z. MicroRNA-761 suppresses remodeling of nasal mucosa and epithelial-mesenchymal transition in mice with chronic rhinosinusitis through LCN2. Stem Cell Res Ther. 2020 Apr 9;11(1):151.
27. Yang N, Cheng H, Mo Q, Zhou X, Xie M. miR-155-5p downregulation inhibits epithelial-to-mesenchymal transition by targeting SIRT1 in human nasal epithelial cells. Mol Med Rep. 2020 Nov;22(5):3695-3704.
28. Li X, Li C, Zhu G, Yuan W, Xiao ZA. TGF-β1 induces epithelial-mesenchymal transition of chronic sinusitis with nasal polyps through MicroRNA-21. Int Arch Allergy Immunol. 2019;179(4):304-319.
29. Gan J, Liu S, Zhang Y, et al. MicroRNA-375 is a therapeutic target for castration-resistant prostate cancer through the PTPN4/STAT3 axis. Exp Mol Med, 2022,54(8):1290-1305.
30. Pillman K A, Phillips C A, Roslan S, et al. miR-200/375 control epithelial plasticity-associated alternative splicing by repressing the RNA-binding protein Quaking. EMBO J, 2018,37(13).
31. Wang S, Tong X, Li C, et al. Quaking 5 suppresses TGF-beta-induced EMT and cell invasion in lung adenocarcinoma. EMBO Rep, 2021,22(6):e52079.
32. He S, Wu J, Han D, et al. Differential expression profile of plasma exosomal microRNAs in chronic rhinosinusitis with nasal polyps. Exp Biol Med (Maywood), 2022,247(12):1039-1046.
33. Choi E B, Hong S W, Kim D K, et al. Decreased diversity of nasal microbiota and their secreted extracellular vesicles in patients with chronic rhinosinusitis based on a metagenomic analysis. Allergy, 2014,69(4):517-526.
34. Nocera A L, Mueller S K, Stephan J R, et al. Exosome swarms eliminate airway pathogens and provide passive epithelial immunoprotection through nitric oxide. J Allergy Clin Immunol, 2019,143(4):1525-1535.
35. Mueller S K, Nocera A L, Dillon S T, et al. Noninvasive exosomal proteomic biosignatures, including cystatin SN, peroxiredoxin-5, and glycoprotein VI, accurately predict chronic rhinosinusitis with nasal polyps. Int Forum Allergy Rhinol, 2019,9(2):177-186.
36. Nocera AL, Miyake MM, Seifert P, Han X, Bleier BS. Exosomes mediate interepithelial transfer of functional P-glycoprotein in chronic rhinosinusitis with nasal polyps. Laryngoscope. 2017 Sep;127(9):E295-E300.
37. Cha S, Seo E H, Lee S H, et al. MicroRNA expression in extracellular vesicles from nasal lavage fluid in chronic rhinosinusitis. Biomedicines, 2021,9(5).
38. Ren Z, Lv M, Yu Q, Bao J, Lou K, Li X. MicroRNA-370-3p shuttled by breast cancer cell-derived extracellular vesicles induces fibroblast activation through the CYLD/Nf-κB axis to promote breast cancer progression. FASEB J. 2021 Mar;35(3):e21383.
39. Ren W, Hou J, Yang C, et al. Extracellular vesicles secreted by hypoxia pre-challenged mesenchymal stem cells promote non-small cell lung cancer cell growth and mobility as well as macrophage M2 polarization via miR-21-5p delivery. J Exp Clin Cancer Res, 2019,38(1):62.
40. Wang T, Chen D, Wang P, Xu Z, Li Y. miR-375 prevents nasal mucosa cells from apoptosis and ameliorates allergic rhinitis via inhibiting JAK2/STAT3 pathway. Biomed Pharmacother. 2018 Jul;103:621-627.
41. Ji Y, Yang X, Su H. Overexpression of microRNA-375 impedes platelet-derived growth factor-induced proliferation and migration of human fetal airway smooth muscle cells by targeting Janus kinase 2. Biomed Pharmacother. 2018 Feb;98:69-75.
42. Bleck B, Grunig G, Chiu A, et al. MicroRNA-375 regulation of thymic stromal lymphopoietin by diesel exhaust particles and ambient particulate matter in human bronchial epithelial cells. J Immunol, 2013,190(7):3757-3763.
43. van Nijnatten J, Brandsma C A, Steiling K, et al. High miR203a-3p and miR-375 expression in the airways of smokers with and without COPD. Sci Rep, 2022,12(1):5610.
44. He L, Liu J, Wang X, Wang Y, Zhu J, Kang X. Identifying a novel serum microRNA biomarker panel for the diagnosis of childhood asthma. Exp Biol Med (Maywood). 2022 Oct;247(19):1732-1740.
45. Luo X, Zeng Q, Yan S, Liu W, Luo R. MicroRNA-375-mediated regulation of ILC2 cells through TSLP in allergic rhinitis. World Allergy Organ J. 2020 Aug 9;13(8):100451.
46. Rezaei R, Baghaei K, Amani D, et al. Exosome-mediated delivery of functionally active miRNA-375-3p mimic regulate epithelial mesenchymal transition (EMT) of colon cancer cells. Life Sci, 2021,269:119035.
47. Zhao J F, Zhao Q, Hu H, et al. The ASH1-miR-375-YWHAZ signaling axis regulates tumor properties in hepatocellular carcinoma. Mol Ther Nucleic Acids, 2018,11:538-553.
48. 76 Martínez-Terroba E, Behrens C, de Miguel F J, et al. A novel protein-based prognostic signature improves risk stratification to guide clinical management in early-stage lung adenocarcinoma patients. J Pathol, 2018,245(4):421-432.
49. Han J, Meng J, Chen S, et al. YY1 complex promotes quaking expression via super-enhancer binding during EMT of hepatocellular carcinoma. Cancer Res, 2019,79(7):1451-1464.
50. Chu L, Hu Y, Jiang YH, Xu C, Liu WC, Lu ZF. Effects of RNA binding protein QKI on pancreatic cancer ductal epithelial cells and surrounding activation fibroblasts. J Cell Biochem. 2019 Jul;120(7):11551-11561.

Qintai Yang, M.D., Ph.D.
Department of Otolaryngology
Head and Neck Surgery
The Third Affiliated Hospital of Sun Yat-Sen University
No. 600 Tianhe Road
Guangdong
Guangzhou 510630
China

Tel: +86-20-85253045
E-mail: yangqint@mail.sysu.edu.cn

Yana Zhang, M.D., Ph.D.
Department of Otolaryngology
Head and Neck Surgery
The Third Affiliated Hospital of Sun Yat-Sen University
No. 600 Tianhe Road
Guangdong
Guangzhou 510630
China

Tel: +86-20-85253045
E-mail: zhangyn95@mail.sysu.edu.cn

Xinyue Wang[1,2,$], Rui Zheng[1,2,$], Weicheng Liang[3,4], Huijun Qiu[1,2], Tian Yuan[1,2], Weihao Wang[1,2], Huiyi Deng[1,2], Weifeng Kong[1,2], Jingyuan Chen[1,2], Yurong Bai[1,2], Yue Li[1], Yubin Chen[1,2], Qingwu Wu[1,2], Shuo Wu[1,2], Xuekun Huang[1,2], Zhaohui Shi[1,2], Qingling Fu[5,6], Yana Zhang[1,2,#], Qintai Yang[1,2,#]

[1] Department of Otolaryngology-Head and Neck Surgery, The Third Affiliated Hospital of Sun Yat-Sen University, Guangzhou, China
[2] Department of Allergy, The Third Affiliated Hospital of Sun Yat-Sen University, Guangzhou, China
[3] Department of Biotherapy Center, The Third Affiliated Hospital of Sun Yat-sen University, Guangzhou, China
[4] Cell-gene Therapy Translational Medicine Research Center, The Third Affiliated Hospital of Sun Yat-sen University, Guangzhou, China
[5] Otorhinolaryngology Hospital, The First Affiliated Hospital, Sun Yat-sen University, Guangzhou, China
[6] Key Laboratory for Stem Cells and Tissue Engineering, Ministry of Education, Sun Yat-sen University, Guangzhou, China

***Received for publication:** Decvember 26, 2023
Accepted: March 13, 2024

Associate Editor:
Sietze Reitsma

[$] contributed equally to the work

[#] contributed equally to the design and supervision

This manuscript contains online supplementary material

SUPPLEMENTARY MATERIAL

Methods

Ethics

This study was approved by the Ethics Committee of the Third Affiliated Hospital of Sun Yat-Sen University (File No. RG2023-124-01) and conducted with written informed consent from all participants. The diagnostic criteria of CRSwNP were according to the European Position Paper on Rhinosinusitis and Nasal polyps 2020 [1]. When the average percentage of eosinophils exceeds 10% of the total inflammatory cells in nasal tissue, it was defined as ENP; otherwise, it was defined as nonENP [2, 3]. A total of 37 ENP patients, 34 nonENP patients, and 26 control subjects undergoing septoplasty because of anatomical factors were included in this study for experiments. All subjects received surgical treatment at the Third Affiliated Hospital of Sun Yat-Sen University during the period from October 2019 to Jan 2023, without being treated with systemic corticosteroids within 4 weeks before surgery, and their nasal tissues were collected as biopsy specimens during surgery. Patients with uncontrolled systemic diseases, immunodeficiency, fungal sinusitis, and pregnancy were excluded. The SinoNasal Outcomes Test 22 (SNOT22), visual analogue scale (VAS), and Lund-Mackay scoring system were used to assess disease severity. Besides, the Sniffin' Sticks test, threshold discrimination identification score (TDI), and questionnaire of olfactory disorders negative statements (QOD-NS) were utilized to evaluate olfactory function.
Atopy status was assessed by skin prick test and/or specific IgE against common inhalant allergens detected by using the ImmunoCAP. Allergic rhinitis is diagnosed according to Chinese guideline for diagnosis and treatment of allergic rhinitis [4]. The diagnosis of asthma was made according to the Global Initiative for Asthma guideline [5]. The patients' characteristics are presented in Table S1. Not all samples were included in every experiment protocol because of the limited quantity.

Isolation of extracellular vesicles (EVs) from nasal mucosa

EVs from nasal mucosa were isolated as previously reported [6, 7]. The Dulbecco's Phosphate-Buffered Saline (DPBS, Sigma, USA) used during this study was filtered through 0.22μm filters (PALL, USA). After removing blood and residual bone, nasal tissues were washed with cold DPBS three times. Then, tissues were gently minced into small pieces and digested with collagenase type II (2 mg/mL, Roche, Switzerland) and Deoxyribonuclease I (0.1 mg/mL, Roche, Switzerland) at 37°C with stirring for 1 hour [8]. After a grind and filtration step (70μm cell filter, Biologix, China), cells debris was eliminated by centrifugation at 300x g for 10 minutes, 2,000x g for 20 minutes, and 9,000x g for 20 minutes, sequentially. Then, supernatants were centrifuged at 13,000x g for 1 hour and 11,8000x g for 2.5 hours to collect median/large (Type 40 Ti rotor, 8,500rpm, k-factor 1279.1, Beckman Coulter, Germany) and small EVs (Type 40 Ti rotor, 25,800rpm, k-factor 178.6, Beckman Coulter, Germany), respectively. All centrifugations were performed at 4°C. EVs-enriched pellets were resuspended in DPBS and undergone further processing.

Western blot (WB) analysis

RIPA lysis buffer with protease inhibitors and phosphatase inhibitors (Beyotime Biotechnology, China) was used to isolate proteins from EVs and cells. Protein concentration was measured through the Enhanced BCA Protein Assay Kit (Beyotime Biotechnology, China). Then, proteins were loaded onto SDS-PAGE gels and transferred to PVDF membranes (Merck Millipore, Germany). The membranes were blocked with 5% Skim Milk (BD Bioscience, USA) in Tris Buffered Saline with Tween (TBST, Servicebio, China) for 1 hour and incubated with primary antibodies at 4°C overnight (antibodies used were listed in Table S2). After being washed 3 times, the membranes were incubated with corresponding secondary antibodies for 1 hour and washed with TBST 3 times. Primary antibodies were diluted in 5% Bovine Serum Albumin (BSA, MP Biomedicals, USA), while secondary antibodies were diluted in 5% Skim Milk (BD Bioscience, USA). Finally, signals were detected and analyzed by FluorChem Western Blot Imaging Systems (ProteinSimple, USA) with the enhanced chemiluminescence detection system (NCM Biotech, China).

EVs identification by transmission electron microscopy, nanoparticle tracking analysis and WB

According to previous research [9], vesicles were investigated by negative staining. Briefly, placed 10μg vesicles onto copper grids, precipitated for 3 minutes, then used filter paper to absorb the floating liquid from the edge of the copper grids. Stained the samples with 10μl phosphotungstic acid for 3 minutes, repeating the step of absorption with filter paper. Dried negative-stained samples at room temperature for 5 minutes and examined on a transmission electron microscope (JEM-1200EX, Japan Electronics Co, Ltd, Japan) at 100kV.
In addition, the size distribution of vesicles was evaluated using a Nanosight NS300 particle size analyzer (Malvern Panalytical Ltd, UK) [10]. After proper dilution, samples were collected in a syringe and slowly advanced into the sample chamber. 3 movie recordings (20×6 magnification, 30 frames per second) were captured and then averaged to measure the size and concentration of EVs. Both positive markers (CD9, CD63 and TSG101) and negative marker (Calnexin) of EVs were measured by WB.

Reverse-transcription quantitative polymerase chain reaction (RT-qPCR)

According to the manufacturer's recommendations, tissue-RNA and EVs-RNA were extracted as previously described [8], and cell/tissue-RNA was extracted by RNA Quick Purification kit (ESscience, China). Stem-loop method (riboSCRIPT Reverse Transcription Kit, RiboBio, China, TB Green Premix Ex Taq II, Takara, Japan) was used for miRNA detection, and RNA input was normalized by human U6 snRNA. MRNA expression was detected by TB green-based RT-qPCR (Takara, Japan). Primers for mature miRNA assays were purchased from RiboBio (Guangzhou, China), others were listed in Table S4. Differences in relative expression were calculated by the 2-ΔΔCt method.

MiRNA sequencing and bioinformatics analysis

MiRNA library construction and sequencing were performed by BGI Genomics (Shenzhen, China). According to the manufacturer's instructions, miRNA was extracted from 3 IT-sEVs, 3 ENP-sEVs and 3 nonENP-sEVs by MiRNasy Mini Kit (QIAGEN, Germany). The library was prepared with 1 μg total RNA for each sample. Total RNA was purified by electrophoretic separation on a 15% urea denaturing polyacrylamide gel electrophoresis (PAGE) gel and small RNA regions corresponding to the 18–30 nt bands in the marker lane (14-30 ssRNA Ladder Marker, TAKARA, Japan) were excised and recovered. MiRNA sequencing was performed on the DNBSEQ platform and SOAPnuke was used to clean tag [11]. After filtering, clean data was mapped to the reference genome and other miRNA databases with Bowtie2 (v2.2.5) software [12]. The miRNA expression level was calculated by counting the absolute number of molecules using unique molecular identifiers. Publicly available algorithms including miRDB (www.mirdb.org), Tarbase (dianalab.e-ce.uth.gr/html/diana/web/index.php?r=tarbasev8), and Targetscan 8.0 (www.targetscan.org/vert_80/) were applied to predict target genes of miR-375-3p.

Dual-luciferase reporter assay

HEK 293T cells (the Cell Bank at the Institute of Biochemistry and Cell Biology, China Academy of Science, China) were cultured in Dulbecco's Modified Eagle's Medium (DMEM, Gibco, USA) supplemented with 10% FBS (ExCell Bio, China) at 37°C under 5% CO_2. Sequence analysis indicated that the 3'- untranslated region (UTR) of QKI mRNA contains three conserved possible biding sites (913-919, 1025-1031, and 2438-2444) for miR-375-3p. Thus, the reporter plasmids containing either wild type (WT) or mutation (MT) versions of the 3'UTR of QKI were prepared. More details of dual-luciferase reporters are listed in Table S5. Next, these different constructs were co-transfected with miR-375-3p mimic (RiboBio, China) into HEK 293T cells using Lipofectamine 3000 (Invitrogen, USA), respectively [13]. According to the manufacturer's instructions, firefly and Renilla luciferase activities were measured 48 hours after transfection using the Dual-Luciferase Reporter Assay System (Promega, USA).

Human nasal epithelial cells (hNECs) culture

HNECs were cultured according to the method as previously published [14]. After careful cleaning with DPBS, tissue from nasal polyps (NP) or inferior turbinate (IT) was chopped up and incubated in Dulbecco's Modified Eagle's Medium: Nutrient Mixture F-12 (DMEM/F-12, Gibco, USA) with Dispase II (Sigma, USA) overnight at 4°C. Removed the solution by centrifugation (1500rpm for 5min), then incubated in 0.05% trypsin at 37°C for 15min. Neutralized trypsin with 10% fetal bovine serum (FBS, ExCell Bio, China). After a filtration (70μm) and a washing step with DPBS (1500rpm for 5min), hNECs were finally cultured in PneumaCult-Ex Medium (Stemcell, Canada), which is serum and BPE-free medium for the expansion of primary airway epithelial cells with the elimination of fibroblasts at 37°C in an atmosphere of 5% CO2 and 95% relative humidity.

Vector construction and transfection experiment

The human gene QKI was generated by PCR amplification from Hep3B cells cDNA library. Then QKI and its mutants were cloned into Dual-Luciferase vectors, respectively. Lentiviral vectors carrying miR-375-3p inhibitor or QKI cDNA/shRNA were purchased from GeneCopoeia (Maryland, USA), while miRNA mimic was purchased from Ribobio (Guangzhou, China). Besides, according to the manufacturer's instructions, Lipofectamine 3000 regent (Invitrogen, USA) was used for stable transfection and riboFectTM CP Transfection Kit (RiboBio, China) was used for transient transfection of miRNA mimic. Viruses were packaged and amplified in HEK 293T cells. After transfection, the supernatant was harvested at 72h and filtered through the fluoride filter (PALL, USA), then concentrated by Universal Virus Concentration Kit (Beyotime, China) and stored at -80°C. More details are listed in Table S4, S5.

SEVs uptake experiment

According to the manufacturer's instruction, sEVs were labelled with PKH67 fluorescent dye (PKH67 fluorescent cell linker kit, Sigma, USA), and cell membrane of hNECs was labelled with Dil dye (1,1'-dioctadecyl-3,3,3',3'-tetramethylindocarbocyanine perchlorate, Invitrogen, USA). Then sEVs (15μg) were added to $1X10^4$ hNECs to monitor sEVs trafficking into hNECs at different time points. HNECs were fixed with 4% paraformaldehyde (Servicebio, China). After washing with PBS three times, hNECs were stained with DAPI (Biolegend, USA) for 5 min. A confocal microscope (Leica STELLARISSTED, Germany) was used to capture images.

Immunofluorescence (IF) and immunohistochemistry (IHC)

IF and IHC were performed as previously reported [14]. For IF, hNECs were fixed with 4% paraformaldehyde (Servicebio, China)

and permeabilized with 0.02% Triton X-100 (Sigma, USA). The permeabilized hNECs were incubated with primary antibodies (listed in Table S2) at 4°C overnight. After washing with PBS, hNECs were incubated with appropriated secondary antibodies (listed in Table S3) at room temperature for 1 hour. DAPI (Biolegend, USA) was used for nuclei staining. Typical images of EMT markers and EVs uptake were acquired by confocal microscope (Leica STELLARISSTED, Germany), while typical images of QKI^+ cells were acquired by fluorescence microscope (NIKON Ti2, Japan).

Paraffin sections (4μm) were prepared from each block as to immunohistochemical staining, epitope retrieval was performed by using EDTA pH 9.0 (Servicebio, China). 3% hydrogen peroxide and 10% goat serum were applied to block endogenous peroxidase activity and non-specific binding, respectively. After incubation with primary antibodies (listed in Table S2) at 4°C overnight, sections were incubated with secondary antibodies labeled horseradish peroxidase (listed in Table S3). Subsequently, sections were incubated in DAB solution (ZSGB-BIO, China), and then were counterstained with hematoxylin solution (Servicebio, China). Images were acquired by fluorescence microscope (NIKON Ti2, Japan).

References

1. Fokkens WJ, Lund VJ, Hopkins C, et al. European Position Paper on Rhinosinusitis and Nasal Polyps 2020. Rhinology, 2020,58(Suppl S29):1-464.
2. Mahdavinia M, Suh LA, Carter RG, et al. Increased noneosinophilic nasal polyps in chronic rhinosinusitis in US second-generation Asians suggest genetic regulation of eosinophilia. J Allergy Clin Immunol, 2015,135(2):576-579.
3. Cao PP, Li HB, Wang BF, et al. Distinct immunopathologic characteristics of various types of chronic rhinosinusitis in adult Chinese. J Allergy Clin Immunol, 2009,124(3):478-484, 481-484.
4. Chinese guideline for diagnosis and treatment of allergic rhinitis (2022, revision). Zhonghua Er Bi Yan Hou Tou Jing Wai Ke Za Zhi, 2022,57(2):106-129.
5. Reddel HK, Bacharier LB, Bateman ED, et al. Global initiative for asthma strategy 2021: executive summary and rationale for key changes. J Allergy Clin Immunol Pract, 2022,10(1S):S1-S18.
6. Crescitelli R, Lasser C, Jang SC, et al. Subpopulations of extracellular vesicles from human metastatic melanoma tissue identified by quantitative proteomics after optimized isolation. J Extracell Vesicles, 2020,9(1):1722433.
7. Kowal J, Arras G, Colombo M, et al. Proteomic comparison defines novel markers to characterize heterogeneous populations of extracellular vesicle subtypes. Proc Natl Acad Sci U S A, 2016,113(8):E968-E977.
8. Zheng R, Wang D, Wang K, et al. Elevated expression of IL-17RB and ST2 on myeloid dendritic cells is associated with a Th2-skewed eosinophilic inflammation in nasal polyps. Clin Transl Allergy, 2018,8:50.
9. Rikkert LG, Nieuwland R, Terstappen L, et al. Quality of extracellular vesicle images by transmission electron microscopy is operator and protocol dependent. J Extracell Vesicles, 2019,8(1):1555419.
10. Gardiner C, Ferreira YJ, Dragovic RA, et al. Extracellular vesicle sizing and enumeration by nanoparticle tracking analysis. J Extracell Vesicles, 2013,2.
11. Chen Y, Chen Y, Shi C, et al. SOAPnuke: a MapReduce acceleration-supported software for integrated quality control and preprocessing of high-throughput sequencing data. Gigascience, 2018,7(1):1-6.
12. Langmead B, Trapnell C, Pop M, et al. Ultrafast and memory-efficient alignment of short DNA sequences to the human genome. Genome Biol, 2009,10(3):R25.
13. Yu X, Zhang Y, Cavazos D, et al. miR-195 targets cyclin D3 and survivin to modulate the tumorigenesis of non-small cell lung cancer. Cell Death Dis, 2018,9(2):193.
14. Li Y, Chang LH, Huang WQ, et al. IL-17A mediates pyroptosis via the ERK pathway and contributes to steroid resistance in CRSwNP. J Allergy Clin Immunol, 2022,150(2):337-351.

Table S1. Clinical characteristics of patients.

	Control	ENP	nonENP
Total subjects enrolled	26	37	34
Methodology used			
EVs isolation			
Subject number	14	20	18
Gender, male	11 (78.57%)	13 (65%)	14 (77.78%)
Age (years)	32.5 (26, 38.75)	38.5 (34, 43.25)	32.5 (25, 53.25)
Patients with atopy	0 (0%)	0 (0%)	1 (5.56%)
Patients with AR	0 (0%)	9 (45%)	2 (11.11%)
Patients with asthma	0 (0%)	4 (20%)	1 (5.56%)
RT-qPCR			
Subject number	10	13	11
Gender, male	10 (100%)	7 (53.85%)	7 (63.64%)
Age (years)	26 (22.5, 32.75)	42 (35, 56)	35 (25. 5,49)
Patients with atopy	0 (0%)	0 (0%)	0 (0%)
Patients with AR	0 (0%)	2 (15.38%)	0 (0%)
Patients with asthma	0 (0%)	0 (0%)	0 (0%)
Ex vivo study			
Subject number	6	9	7
Gender, male	5 (83.33%)	8 (88.89%)	5 (71.43%)
Age (years)	29 (24.25, 35.25)	48 (39, 55)	44 (26, 53.5)
Patients with atopy	0 (0%)	0 (0%)	0 (0%)
Patients with AR	0 (0%)	1 (11.11%)	0 (0%)
Patients with asthma	0 (0%)	2 (22.22%)	0 (0%)

For continuous variables, results were expressed as medians and interquartile ranges. For categorical variables, results were summarized by percentage. EVs, extracellular vesicles; AR, allergic rhinitis; ENP, eosinophilic chronic rhinosinusitis with nasal polyps; nonENP, non-eosinophilic chronic rhinosinusitis with nasal polyps.

Table S2. Primary antibodies.

Antibodies	Manufacturer	Cat.No.	Dilution
WB			
anti-CD9	Abcam	ab236630	1:1000
anti-CD63	Abcam	ab134045	1:1000
anti-TSG101	Abcam	ab125011	1:1000
anti-Calnexin	Abcam	ab133615	1:1000
anti-QKI	Abcam	ab126742	1:2000
anti-ZO-1	Proteintech	21773-1-AP	1:1000
anti-E-Cadherin	CST	14472	1:1000
anti-Vimentin	CST	5741	1:1000
anti-α-SMA	CST	19245	1:1000
anti-GAPDH	CST	2118	1:3000
IF			
anti-QKI	Abcam	ab126742	1:100
anti-ZO-1	Proteintech	21773-1-AP	1:200
anti-E-Cadherin	CST	14472	1:100
anti-Vimentin	Santa Cruz	sc-6260	1:50
anti-α-SMA	CST	19245	1:200
IHC			
anti-ZO-1	Proteintech	21773-1-AP	1:400
anti-E-Cadherin	CST	14472	1:200
anti-Vimentin	CST	5741	1:200
anti-α-SMA	CST	19245	1:200

TSG101, tumor susceptibility gene 101 protein; QKI, KH domain RNA binding protein; α-SMA, α-smooth muscle actin; GAPDH, glyceraldehyde-3-phosphate dehydrogenase; ZO-1, zonula occludens protein 1; CD9, Tetraspanin-29; CD63, CD63 antigen; WB, western blot; IF, immunofluorescence; IHC, immunohistochemistry.

Table S3. Secondary antibodies.

Antibodies	Manufacturer	Cat.No.	Dilution
WB			
Goat anti-rabbit IgG, HRP-link	CST	7074S	1:5000
Goat anti-mouse IgG, HRP-link	CST	7076S	1:5000
IF	Abcam	ab125011	1:1000
Goat anti-Rabbit IgG, Alexa Fluor™ 594	Invitrogen	A11034	1:500
Goat anti-Mouse IgG, Alexa Fluor™ Plus 488	Invitrogen	A32742	1:500
IHC	Proteintech	21773-1-AP	1:1000
Goat anti-rabbit IgG, HRP-link	CST	7074S	1:200
Goat anti-mouse IgG, HRP-link	CST	7076S	1:200

WB, western blotting; IF, immunofluorescence; IHC, immunohistochemistry; HRP, horseradish peroxidase.

Table S4. Primers sequences and vectors construction.

Genes	Primer sequences	Annealing temperature(°C)
RT-qPCR		
QKI	F: AAGCCCACCCCAGATTACCT R: ACTCTGCTAATTTCTTCGTCCAG	60
GAPDH	F: ATCATCCCTGCCTCTACTGG R: GTCAGGTCCACCACTGACAC	60
ELAVL4	F: CGGTGCTACGGAACCGATTAC R: TTGTCCAGCCTGAACCTCTGA	60
PTPN4	F: AGCAGCTAAAGAGAGGATCTCC R: GCAGCAGTATTAGAAGGACAGG	60
MXI1	F: GCGCCTTTGTTTAGAACGCTT R: AATGCTGTCCATTCGTATTCGT	60
RBPJ	F: AACAAATGGAACGCGATGGTT R: GGCTGTGCAATAGTTCTTTCCTT	60
PITPNA	F: ACGAGAAGGACGGTGAGAAAG R: AGTAGGGGTAAGCATTCCAGG	60
RPN1	F: GGCCAAGATTTCAGTCATTGTGG R: CTTCGTTGGATAGGGAGAGTAGA	60
LRAT	F: TGATGCCCGACATCCTGTTG R: ATGTTAGCTCCGTAGGCGAAG	60
KLF5	F: TCAGTCGTAGACCAGTTCTTCA R: CTGGGATTTGTAGAGGCCAGT	60
CHSY1	F: GCTCCGCCATCGCACAATA R: AGCTGGAGGTCCTCTTTATGAAT	60
Vector construction		
QKI-3′UTR-1	F: CTAGCTAGCAAGCCATGCTTGCCTATTTG R: GCGTCGACTGTTTCTTGACAACCACCAGA	58
QKI-3′UTR-2	F: CTAGCTAGCAACCCTGAAGAACGTGACCA R: GCGTCGACAAAGGCAAGTGGCAAGAGAA	59

QKI, KH domain RNA binding; GAPDH, glyceraldehyde-3-phosphate dehydrogenase; ELAVL4, ELAV like RNA binding protein 4; PTPN4, tyrosine-protein phosphatase non-receptor type 4; MXI1, max-interacting protein 1; RBPJ, recombination signal binding protein for immunoglobulin kappa J region; PITPNA, phosphatidylinositol transfer protein alpha; RPN1, ribophorin I; LRAT, lecithin retinol acyltransferase; KLF5, kruppel-like factor 5; CHSY1, Chondroitin synthase-1; UTR, untranslated regions.

Table S5. Vectors target sequences.

Vectors	Target sequences
Luciferase reporter assay	
WT1+2	5′…CAAAUGAACAAAA…AAAAAGAACAAAG…3′
WT3	5′…GCUCUGAACAAAC…3′
MT1	5′…CAAAUCTTGTTAA…3′
MT2	5′… AAAAACTTGTTAG…3′
MT1+2	5′… GCUCUGAACAAAC…CAAAUCTTGTTAA…3′
MT3	5′… GCUCUCTTGTTAC…3′
Transfection	
shQKI	CCGAAGCTGGTTTAATCTATA

QKI, KH domain RNA binding; WT, wild type; MT, mutation.

Table S6. DE-miRNAs in sEVs.

miRNAs	*Log2FC*	*adj* P value
ENP-sEVs vs IT-sEVs		
Up-regulated		
miR-374c-3p	6.90	1.22E-11
miR-302d-3p	12.69	1.32E-08
miR-3184-3p	12.76	1.98E-07
miR-302b-3p	11.95	2.00E-06
miR-302c-3p	11.56	2.54E-05
miR-302a-3p	11.44	5.10E-05
miR-10a-5p	2.59	3.75E-04
miR-9-3p	3.06	4.7E-04
miR-208a-3p	10.79	1.64E-04
miR-9-5p	2.14	1.68E-03
miR-424-5p	3.29	1.79E-03
miR-375-3p	1.91	5.82E-03
miR-429	1.84	5.86E-03
miR-208a-5p	10.25	1.75E-02
Down-regulated		
miR-374b-5p	-3.24	8.09E-05
miR-412-5p	-11.08	8.18E-05
novel-miR-209-3p	-3.59	1.54E-03
miR-139-5p	-1.60	2.03E-03
miR-23b-3p	-1.38	5.86E-03
miR-125b-5p	-1.11	8.67E-03
miR-101-3p	-10.46	1.19E-02
miR-145-5p	-1.34	1.19E-02
miR-1246	-2.50	1.43E-02
novel-miR-261-5p	-10.12	2.12E-02
novel-miR-283-5p	-6.43	2.12E-02
miR-214-5p	-2.21	2.41E-02
nonENP-sEVs vs IT-sEVs		
Up-regulated		
miR-374c-3p	7.35	1.33E-03
miR-34c-3p	2.66	2.37E-02
Down-regulated		
miR-199a-3p	-3.81	1.39E-05
nonENP-sEVs vs ENP-sEVs		
Up-regulated		
miR-412-5p	11.34	1.04E-02

DE-miRNAs, differentially expressed miRNAs; sEVs, small extracellular vesicles; IT, inferior turbinate; ENP, eosinophilic chronic rhinosinusitis with nasal polyps; nonENP, non-eosinophilic chronic rhinosinusitis with nasal polyps.

Table S7. Target genes of miR-375-3p from databases.

Target Gene	Tarbase (Predicted Score)	Targetscan (Cumulative weighted context^{++} score)	miRDB (Target Score)
ELAVL4	1	-0.58	97
PTPN4	0.988	-0.05	71
MXI1	0.937	-0.28	70
RBPJ	0.917	-0.18	93
PITPNA	0.899	-0.15	60
RPN1	0.878	-0.33	56
LRAT	0.872	-0.32	71
KLF5	0.796	-0.16	87
CHSY1	0.783	-0.19	66
QKI	0.731	-0.15	82
GATA6	0.728	-0.12	75
EIF1	0.683	-0.14	69
GMFB	0.65	-0.13	52
JAK2	/	-0.18	66
YWHAZ	/	-0.13	56
ATP1B1	/	-0.21	71
PLEKHA3	/	-0.25	84
ZFP36L2	/	-0.32	91
MPP5	/	-0.05	66
ERC1	/	-0.03	66
UBE3A	/	-0.16	91
WWC2	/	-0.16	64
SLC7A11	/	-0.03	69
XPR1	/	-0.15	59
TCF12	/	-0.14	78
UBE2E2	/	-0.23	72
SPAG9	/	-0.13	94
INSIG2	/	-0.15	50
DIP2C	/	-0.08	87
HAS2	/	-0.14	52
C15orf41	/	-0.17	55
AHR	/	-0.09	67
TNPO3	/	-0.05	76

ELAVL4, ELAV like RNA binding protein 4; PTPN4, tyrosine-protein phosphatase non-receptor type 4; MXI1, max-interacting protein 1; RBPJ, recombination signal binding protein for immunoglobulin kappa J region; PITPNA, phosphatidylinositol transfer protein alpha; RPN1, ribophorin I; LRAT, lecithin retinol acyltransferase; KLF5, kruppel-like factor 5; CHSY1, Chondroitin synthase-1; QKI, KH domain RNA binding; GATA6, GATA binding protein 6; EIF1, eukaryotic translation initiation factor 1; GMFB, glia maturation factor beta; JAK2, janus kinase 2; YWHAZ, tyrosine 3-monooxygenase/tryptophan 5-monooxygenase activation protein zeta; ATP1B1, ATPase Na^+/K^+ transporting subunit beta 1; PLEKHA3, pleckstrin homology domain containing A3; ZFP36L2, ZFP36 ring finger protein like 2; MPP5, membrane palmitoylated protein 5; ERC1, ELKS/RAB6-interacting/CAST family member 1; UBE3A, ubiquitin-protein ligase 3A; WWC2, WW And C2 domain containing 2; SLC7A11, solute carrier family 7 member 11; XPR1, xenotropic and polytropic retrovirus receptor 1; TCF12, transcription factor 12; UBE2E2, ubiquitin conjugating enzyme E2 E2; SPAG9, sperm associated antigen 9; INSIG2, insulin induced gene 2; DIP2C, disco-interacting protein 2 C; HAS2, hyaluronan synthase 2; C15orf41, chromosome 15 open reading frame 41; AHR, aryl hydrocarbon receptor; TNPO3, transportin 3.

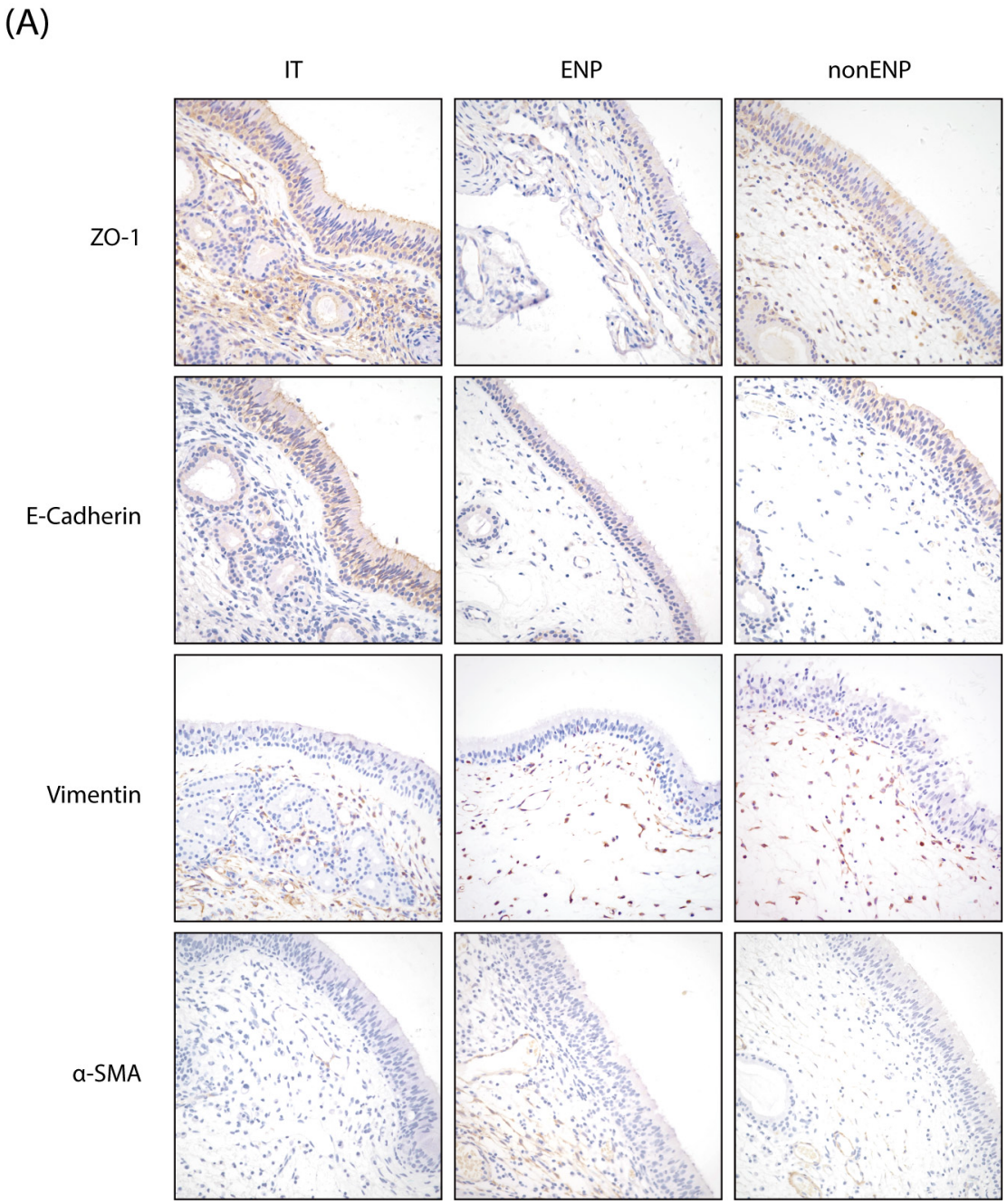

Figure S1. The expression level of EMT markers in different study groups. A, Representative photomicrographs of ZO-1, E-Cadherin, Vimentin, and α-SMA in nasal tissue of control subjects, patients with ENP or nonENP. (×400 magnification). Scale bar, 10μm.

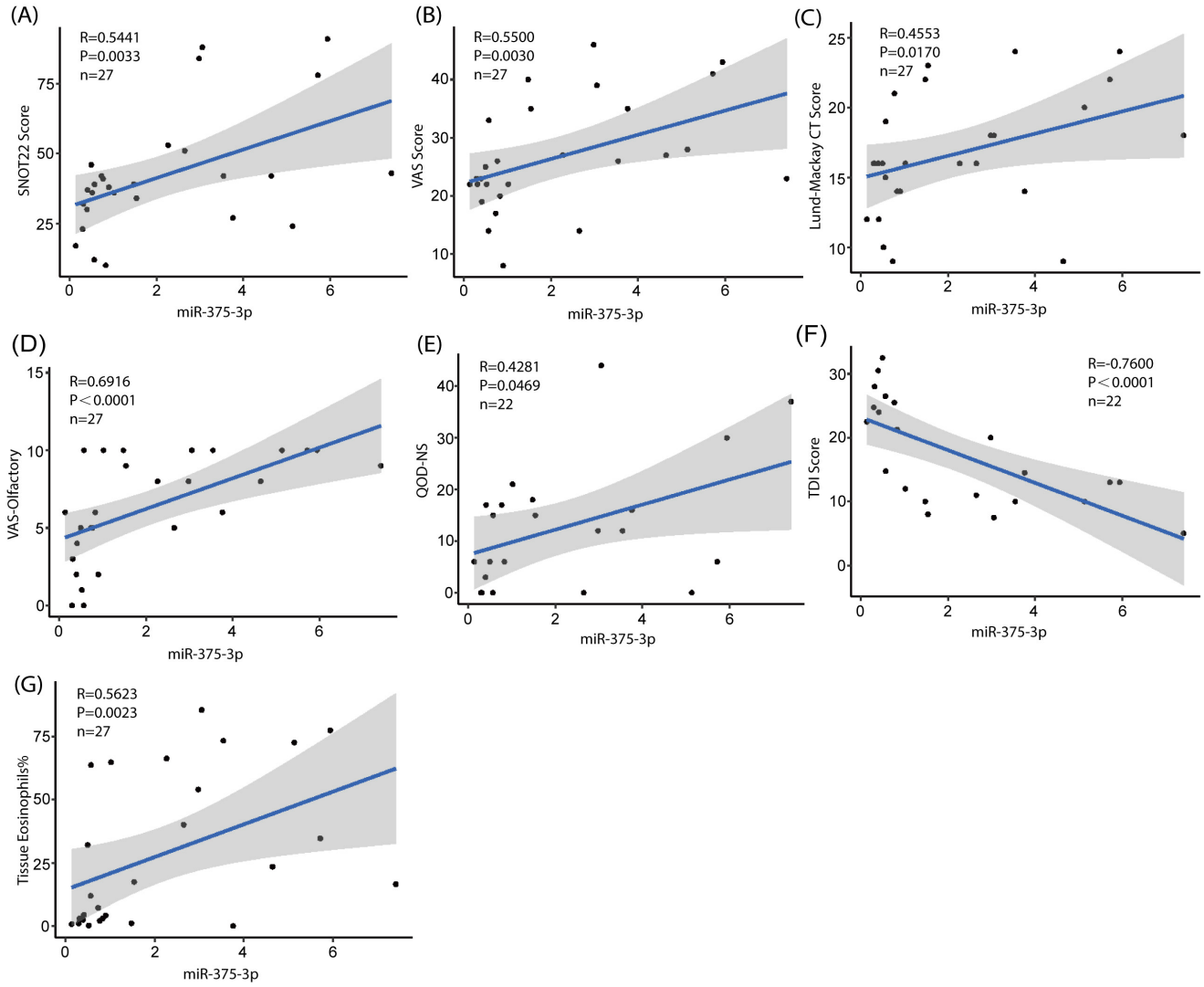

Figure S2. MiR-375-3p derived in NP-sEVs correlates with CRSwNP severity. Correlations between miR375-3p and SNOT22 score (A), VAS score (B), Lund-Mackay CT score (C), olfactory single item in VAS score (D), QOD-NS score (E), TDI score (F), and tissue eosinophil percentage (G).